

University of Windsor

Scholarship at UWindor

Electronic Theses and Dissertations

Theses, Dissertations, and Major Papers

2-1-2022

The Role of Pier Shape and Aspect Ratio on Local Scour with and Without Sacrificial Piles

Mohamed Kharbeche
University of Windsor

Follow this and additional works at: <https://scholar.uwindsor.ca/etd>



Part of the [Civil Engineering Commons](#)

Recommended Citation

Kharbeche, Mohamed, "The Role of Pier Shape and Aspect Ratio on Local Scour with and Without Sacrificial Piles" (2022). *Electronic Theses and Dissertations*. 8791.
<https://scholar.uwindsor.ca/etd/8791>

This online database contains the full-text of PhD dissertations and Masters' theses of University of Windsor students from 1954 forward. These documents are made available for personal study and research purposes only, in accordance with the Canadian Copyright Act and the Creative Commons license—CC BY-NC-ND (Attribution, Non-Commercial, No Derivative Works). Under this license, works must always be attributed to the copyright holder (original author), cannot be used for any commercial purposes, and may not be altered. Any other use would require the permission of the copyright holder. Students may inquire about withdrawing their dissertation and/or thesis from this database. For additional inquiries, please contact the repository administrator via email (scholarship@uwindsor.ca) or by telephone at 519-253-3000ext. 3208.

THE ROLE OF PIER SHAPE AND ASPECT RATIO ON LOCAL SCOUR WITH AND WITHOUT SACRIFICIAL PILES

By

Mohamed Kharbeche

A Thesis
Submitted to the Faculty of Graduate Studies
through the Department of Civil and Environmental Engineering
in Partial Fulfillment of the Requirements for
the Degree of Master of Applied Science
at the University of Windsor

Windsor, Ontario, Canada

2022

© 2022 Mohamed Kharbeche

**EFFECT OF PIER SHAPE AND ASPECT RATIO ON LOCAL SCOUR WITH
AND WITHOUT SACRIFICIAL PILES**

by

Mohamed Kharbeche

APPROVED BY:

V. Roussinova
Department of Mechanical, Automotive and Materials Engineering

T. Bolisetti
Department of Civil and Environmental Engineering

R. Balachandar, Co-Advisor
Department of Civil and Environmental Engineering

P. Williams, Co-Advisor
Department of Civil and Environmental Engineering

January 27, 2022

DECLARATION OF ORIGINALITY

I hereby certify that I am the sole author of this thesis and that no part of this thesis has been published or submitted for publication.

I certify that, to the best of my knowledge, my thesis does not infringe upon anyone's copyright nor violate any proprietary rights and that any ideas, techniques, quotations, or any other material from the work of other people included in my thesis, published or otherwise, are fully acknowledged in accordance with the standard referencing practices. Furthermore, to the extent that I have included copyrighted material that surpasses the bounds of fair dealing within the meaning of the Canada Copyright Act, I certify that I have obtained a written permission from the copyright owner(s) to include such material(s) in my thesis and have included copies of such copyright clearances to my appendix.

I declare that this is a true copy of my thesis, including any final revisions, as approved by my thesis committee and the Graduate Studies office, and that this thesis has not been submitted for a higher degree to any other University or Institution.

ABSTRACT

The complexity of the scour process around bridge piers leads to uneconomical pier design and unnecessary costs. This is due to the current scour estimation methods, which over-predict scour depth. Several aspects of scour have not been fully considered in pier design and require further investigation, such as the pier shape and aspect ratio. Further, scour countermeasures are used to protect the pier and reduce the scour depth. The first objective of the present investigation is to study the combined effects of pier nose shape and aspect ratio on scour geometry. The second objective is to better understand the effect of two different sacrificial piles arrays located in front of the piers in reducing scour. Experiments were carried out with different pier shapes and aspect ratios. The shapes used were round-nosed, sharp-nosed, round-edged, and square for piers with three aspect ratios ($L/a = 1, 2, \text{ and } 4$). In addition, two triangular sacrificial pile arrays were used to study the role of sacrificial piles on scour reduction. The sharp-nosed pier with $L/a = 4$ recorded the minimum scour depth. Moreover, three sacrificial piles in a triangular arrangement resulted in maximum scour reduction. A new scour estimation method was developed using the present investigation and previous experimental results. The separation velocity, the pier shape, and aspect ratio were incorporated into the equation. These parameters were examined and found to be significant factors affecting scour.

DEDICATION

To Dad, Mom, Ines, and Ibrahim

ACKNOWLEDGEMENT

I want to express my sincere thanks to my supervisors, Dr. Ramaswami Balachandar and Dr. Priscilla Williams, for their guidance, support, and help over the past two years. I would also like to thank the members of my evaluation committee, Dr. Tirupati Boliseti, Dr. Vesselina Roussinova, and Dr. Faouzi Gherib, for their comments and suggestions.

My sincere thanks to Dr. Ronald Barron and Dr. Kohei Fukuda for their weekly support and countless help.

I want to thank MITACS Globalink for giving me the opportunity to be in Canada and pursue my M.A.Sc at the University of Windsor.

I would like to extend my appreciation to Mr. Matthew St. Louis, Mr. Jerome Finnerty, and Mr. Ram Barakat for their assistance and expertise in the lab.

With appreciation, I would like to thank all my friends and colleagues: Nimesh Virani, Subhadip Das, Mia Marrocco, Saikrishna Muppavarapu, Maziar Mosavati, Corey Klinkhamer, and Yuanming Yu for helping me whenever I needed them; Motaz Bouabsa, Amine Bejaoui, Yasmine Loussaief, and Alaa Adouani for their friendship, encouragement, and belief.

Finally, I would like to thank my parents, Mohamed Hedi and Najoua Kharbeche, my sister Ines Kharbeche, my brother Ibrahim Kharbeche, and my whole family for their love, support, and guidance.

TABLE OF CONTENTS

DECLARATION OF ORIGINALITY	iii
ABSTRACT	iv
DEDICATION	v
ACKNOWLEDGEMENT	vi
LIST OF TABLES	ix
LIST OF FIGURES.....	x
LIST OF ABBREVIATIONS	xiii
INTRODUCTION.....	1
1.1. Introduction	1
1.2. Objectives.....	4
1.3. Outline of the Thesis	4
LITERATURE REVIEW	6
2.1. General Remarks on Scour Process	6
2.2. Parameters Affecting Scour	7
2.3. Pier Effects	8
2.3.1. Pier Width and Arrangement.....	8
2.3.2. Pier Shape.....	9
2.3.3. Elongated Pier	11
2.4. Bridge Pier Countermeasures.....	13
2.4.1. Efficiency of Countermeasures	14
2.4.2. Collars	14
2.4.3. Sacrificial Piles.....	15
METHODOLOGY	19
3.1. Experimental Set-Up.....	19
3.2. Bed Material	19
3.3. Experimental Procedures.....	19
3.4. Flow Measurements	20
3.5. Experimental Program.....	21
RESULTS AND DISCUSSION	30
4.1. Approach Flow Analysis.....	30

4.2. Scour Analysis.....	31
4.2.1. Series A: Investigation of Pier Shape and L/a Ratio on Scour Depth.....	31
4.2.1.1. Investigation of Pier Shape on Scour Depth	32
4.2.1.2. Investigation of L/a Ratio on Scour Depth.....	33
4.2.2. Investigation of Scour Reduction using Sacrificial Piles	34
4.2.2.1. Series B: Study of Scour Reduction using Five Sacrificial Piles	34
4.2.2.2 Series C: Study of Scour Reduction using Three Sacrificial Piles.....	36
4.2.2.3 Comparison between Series B and Series C Experiments	38
4.3. Development of a New Scour Estimation Method.....	40
CONCLUSIONS AND RECOMMENDATIONS.....	59
5.1. Conclusions	59
5.2. Recommendations	60
REFERENCES.....	61
VITA AUCTORIS	65

LIST OF TABLES

Table 2.1: Pier shape factor K_{sh} values (Obeid and Al-Shukur, 2016)	10
Table 2.2: Measured scour depth of different pier shapes with three different flow velocities (Obeid and Al-Shukur, 2016)	11
Table 3.1. Dimensionless parameters in all the experiments	22
Table 3.2: Experimental program.....	23
Table 4.1: Shear stress velocities for the different tests with various pier shapes, L/a , and N_p	31
Table 4.2: Series A experimental results.....	32
Table 4.3: Series B experimental results	35
Table 4.4: Series C experimental results	37
Table 4.5: Comparison between Series B and Series C results and scour reduction percentage in Series C compared to Series B	39

LIST OF FIGURES

Figure 1.1: Scour-related bridge failure in Alberta, Canada (CTV News, 2013)	5
Figure 2.1: Description of flow structures around a pier (Hodi, 2009).....	17
Figure 2.2: Collar (Plan and side views) (Tafarojnoruz et al., 2012).....	18
Figure 2.3: Schematic of the sacrificial piles in a transverse arrangement (Tafarojnoruz et al., 2012).....	18
Figure 3.1: Schematic of the horizontal laboratory flume used for the experiments (modified from (Williams, 2019))	24
Figure 3.2: Streamwise velocity profiles in the presence and in the absence of the 3 mm rod placed in the sand bed.....	24
Figure 3.3: ASTM sieve analysis for bed sediment used in the experiments	25
Figure 3.4: Point measurements of a centerline profile	25
Figure 3.5: Location of the ADV and LDV for the tests in the absence of the pier.....	26
Figure 3.6: Location of the ADV for tests with 5 and 3 sacrificial piles (B6, B7, B8, C8, C9, and C10).....	26
Figure 3.7: Location of the ADV for the tests (A4, A8, A9, and A10) to get the separation velocity.....	27
Figure 3.8: Different pier shapes and L/a ratios.....	28
Figure 3.9: Schematic of the five sacrificial piles used in Series B	29
Figure 3.10: Schematic of the three sacrificial piles used in Series C	29
Figure 4.1: Streamwise velocity U profiles for tests B6, B7, and B8 with five sacrificial piles compared to tests E and L in the absence of the pier	43
Figure 4.2: Streamwise velocity U profiles for tests C8, C9, and C10 with three sacrificial piles compared to tests E and L in the absence of the pier	43
Figure 4.3: Reynolds shear stress profiles for tests B6, B7, and B8 with five sacrificial piles compared to test E in the absence of the pier	44
Figure 4.4: Reynolds shear stress profiles for tests C8, C9, and C10 with three sacrificial piles compared to test E in the absence of the pier	44
Figure 4.5: Centerline profiles of the piers with $L/a = 1$ (A1, A2, A3, and A4).....	45
Figure 4.6: Centerline profiles of the piers with $L/a = 2$ (A5, A6, and A7).....	45
Figure 4.7: Centerline profiles of the piers with $L/a = 4$ (A8, A9, and A10).....	46

Figure 4.8: Contour profiles of the piers with $L/a = 1$ (A1, A2, A3, and A4)46

Figure 4.9: Contour profiles of the piers with $L/a = 2$ (A5, A6, and A7)47

Figure 4.10: Contour profiles of the piers with $L/a = 4$ (A8, A9, and A10)47

Figure 4.11: Centerline profiles of round-nosed piers (A1: $L/a = 1$, A5: $L/a = 2$, and A8: $L/a = 4$)
.....48

Figure 4.12: Centerline profiles of sharp-nosed piers (A2: $L/a = 1$, A6: $L/a = 2$, and A9: $L/a = 4$)
.....48

Figure 4.13: Centerline profiles of round-edged piers (A3: $L/a = 1$, A7: $L/a = 2$, and A10: $L/a = 4$)
.....49

Figure 4.14: Contour profiles of round-nosed piers (A1: $L/a = 1$, A5: $L/a = 2$, and A8: $L/a = 4$).49

Figure 4.15: Contour profiles of sharp-nosed piers (A2: $L/a = 1$, A6: $L/a = 2$, and A9: $L/a = 4$) .50

Figure 4.16: Contour profiles of round-nosed piers (A3: $L/a = 1$, A7: $L/a = 2$, and A10: $L/a = 4$)
.....50

Figure 4.17: Centerline profiles for piers with $L/a = 2$ with and without five sacrificial piles (tests A5, A6, and A7 without sacrificial piles, and tests B5, B6, and B7 with five sacrificial piles)51

Figure 4.18: Centerline profiles for piers with $L/a = 4$ with and without five sacrificial piles (tests A8, A9, and A10 without sacrificial piles, and tests B8, B9, and B10 with five sacrificial piles) 51

Figure 4.19: Contour profiles for piers with $L/a = 2$ with and without five sacrificial piles (tests A5, A6, and A7 without sacrificial piles, and tests B5, B6, and B7 with five sacrificial piles)52

Figure 4.20: Contour profiles for piers with $L/a = 4$ with and without five sacrificial piles (tests A8, A9, and A10 without sacrificial piles, and tests B8, B9, and B10 with five sacrificial piles).52

Figure 4.21: Centerline profiles for piers with $L/a = 2$ with and without three sacrificial piles (tests A5, A6, and A7 without sacrificial piles, and tests C5, C6, and C7 with three sacrificial piles)53

Figure 4.22: Centerline profiles for piers with $L/a = 4$ with and without three sacrificial piles (tests A8, A9, and A10 without sacrificial piles, and tests C8, C9, and C10 with three sacrificial piles)53

Figure 4.23: Contour profiles for piers with $L/a = 2$ with and without three sacrificial piles (tests A5, A6, and A7 without sacrificial piles, and tests C5, C6, and C7 with three sacrificial piles)...54

Figure 4.24: Contour profiles for piers with $L/a = 4$ with and without three sacrificial piles (tests A8, A9, and A10 without sacrificial piles, and tests C8, C9, and C10 with three sacrificial piles)54

Figure 4.25: Centerline profiles for $L/a = 2$ in Series B and Series C with five and three sacrificial piles (tests: B5, B6, and B7 with five sacrificial piles, and tests C5, C6, and C7 with three sacrificial piles)55

Figure 4.26: Centerline profiles for $L/a = 4$ in Series B and Series C with five and three sacrificial piles (tests: B8, B9, and B10 with five sacrificial piles, and tests C8, C9, and C10 with three sacrificial piles)55

Figure 4.27: Contour profiles for piers with $L/a = 2$ in Series B and Series C with five and three sacrificial piles (tests B5, B6, and B7 with five sacrificial piles, and tests C5, C6, and C7 with three sacrificial piles)56

Figure 4.28: Contour profiles for piers with $L/a = 4$ in Series B and Series C with five and three sacrificial piles (tests B8, B9, and B10 with five sacrificial piles, and tests C8, C9, and C10 with three sacrificial piles)56

Figure 4.30: Separation velocity profiles for different pier shapes and L/a ratios.....57

Figure 4.30: Equilibrium scour depth alteration with L/a57

Figure 4.31: Measured vs predicted d_{se}/a values grouped by investigation using Equation 4.7....58

Figure 4.32: Measured vs predicted d_{se}/a values grouped by investigation using HEC-18 equation58

LIST OF ABBREVIATIONS

a	Transverse pier width
a/b	Blockage ratio
a/d_{50}	Relative coarseness
Al	Alignment of the pier with respect to the approach flow
b_p	Projected width of the pier
d_{50}	Median sediment diameter
D_p	Sacrificial pile diameter
d_{se}	Equilibrium scour depth
d_{se}/a	Relative scour depth
F_d	Densimetric Froude number
F_r	Froude number
g	Acceleration due to gravity
h	Water depth
h/a	Flow shallowness
h_c	Distance between the collar and the surface of water
K_1	Correction factor for pier shape
K_2	Correction factor for the angle of attack of flow
K_3	Correction factor for bed condition
K_4	Armoring condition factor
K_{sh}	Pier shape factor
L	Pier length
L/a	Pier aspect ratio
N_p	Sacrificial pile number
r_{de}	Scour reduction
Re	Reynolds number
Sh	Pier shape
S_{mp}	The lateral spacing between the main piers
S_p	The horizontal spacing between the sacrificial piles
t^*	Equilibrium time scale
U	Streamwise velocity

U/U_c	Flow intensity
U_c	Critical velocity
U_e	Maximum streamwise velocity
U_s	Separation velocity
U_τ	Shear velocity
w_c	Collar width
X_p	Distance between the sacrificial piles and the main pier
α	The wedge of pile group angle
θ	Angle of attack
ϑ	Kinematic viscosity
ρ	Fluid density
ρ_s	Sediment density
σ_g	Uniformity of particle size distribution
τ_w	Wall shear stress

CHAPTER 1

INTRODUCTION

1.1. Introduction

Scour is one of the leading reasons for hydraulic engineering infrastructure failure, especially bridges. The structural integrity is affected by the removed sediment from the immediate vicinity of the foundation of bridge piers and the subsequent lateral support reduction. This is due to the fluid flow interaction with the structure. In North America, more than 50% of bridge failures are due to scour or scour-related complications. Shirhole and Holt (1991) investigated more than 800 bridge collapses in the USA and found that 60% of failures were related to channel-bed scour around bridge piers and channel instability (Melville and Coleman, 2000). In addition, bridge failure brings additional costs and unexpected expenses due to the cost of replacing or repairing the bridge's damaged components. For example, Padgett et al. (2008) studied the cost of bridge damage and repair due to hurricane Katrina, and reported that the Chef Menteur Bridge over Lake Pontchartrain between New Orleans and Slidell, Louisiana collapsed primarily due to scour and erosion of the abutment. The cost to repair the bridge was estimated to be around US \$ 3.6 million.

Similar bridge failures have occurred in the past in Canada. For instance, in 2013, heavy rainfall resulted in extreme flooding and the collapse of a Canadian Pacific Railway bridge over the Bow River in Alberta, due to scour, as shown in **Figure 1.1**. Six train cars were derailed, although no injuries were reported. According to the authorities, the scouring occurred at the bottom of one of the bridge's piers and made it impossible to inspect and detect the problem (CTV News, 2013).

In river channels scouring is described as the erosion of the sediment bed by changes in flow action. Sediment is transported by the flow due to the hydrodynamic forces in the flow field. Scour can be classified as either general or local scour. General scour occurs when the sediment transport happens in the absence of an obstruction in the channel, due to a change in flow velocity or channel characteristics. Local scour occurs in the presence of an obstacle, such as pipelines, sluice gates abutments, and bridge piers. Bridge piers are a common obstacle to the flow in erodible river. The presence of a bridge pier results in diverting the oncoming flow and thereby transporting the sediment. Consequently, scour holes develop by increasing local

sediment transport around the pier. Further, the local scour can be characterized as live-bed or clear-water scour. The live-bed condition occurs when the streamwise velocity U exceeds the critical velocity U_c . The clear-water scour occurs when the streamwise velocity U is less than U_c (Melville and Coleman, 2000).

Numerous investigations have studied local scour around bridge piers to understand the parameters that affect scour. Researchers have investigated the approach flow, the velocity distributions around the pier, the horseshoe vortex upstream of the pier and the wake vortices in the downstream region. Different flow measurement techniques have been used to investigate the flow field surrounding a bridge pier under local scour conditions, such as particle image velocimetry (PIV), laser Doppler velocimetry (LDV), and acoustic Doppler velocimetry (ADV). Further, scour has also been studied using computational methods.

Despite the extensive investigations on scour around bridge piers, fewer studies have been carried out using pier shapes that are not cylindrical to investigate the scour geometry as well as the turbulence features (Vijayasree et al., 2017). The non-circular piers increase the complexity in predicting scour depth due to the modified flow field and the complicated interactions between the approach flow and the elongated piers. Moreover, fewer studies have investigated the effect of the length to width (L/a) ratio of the pier on scour depth.

Scour is highly prioritized in bridge pier design due to its prevalence as a cause of bridge failure. Many scour estimation methods are empirical equations based on laboratory and field experiments. However, these equations over-predict scour depth due to its complexity. Furthermore, many scour prediction methods were developed for particular pier types. For instance, some scour prediction methods do not consider the effect of the pier nose shape. This shows that many aspects of the scour prediction still need to be clarified.

The HEC-18 or CSU equation is the leading scour estimation method for North American bridge pier design. The equation uses K correction factors, as shown in **Equation 1.1**, and it takes into consideration the pier shape factor K_l or K_{sh} , for differing simple pier shapes. The method can be applied to both live-bed and clear-water conditions (Ettema et al., 2011). The effects of pier aspect ratio are incorporated into the HEC-18 equation through the pier skewness factor, which is selected based on the L/a ratio; however, the effects of L/a are not explicitly

incorporated outside of this factor. This method rarely under-predicts scour, but it does show an unnecessarily high estimation, which can lead to costly designs (Guo, 2012).

$$\frac{d_{se}}{a} = 2K_1K_2K_3K_4 \left(\frac{h}{a}\right)^{0.35} F_r^{0.43} \quad [1.1]$$

In **Equation 1.1**, K_1 is the correction factor for pier nose shape, K_2 is the correction factor for the angle of attack of flow, K_3 is the correction factor for bed condition, and K_4 (added to the equation in 2001) is intended to adjust the relative scour depth based on armoring conditions by bed material size.

In general, the over-prediction of scour is not significant for small piers used in laboratory experiments compared to wider piers used in the field. Despite this, the currently used scour equations are largely laboratory data driven. Therefore, an updated equation is required to avoid the unnecessary high prediction and the uneconomical design due to the pier construction and material costs associated with overprediction. At the University of Windsor, Williams (2014) carried out experiments to develop a new scour estimation method based on the previous investigations and findings realized at the university. It was found that the densimetric Froude number and the effect of blockage significantly affected the scour depth. However, the developed equation neglects the pier shape and the aspect ratio (L/a) effects. These two parameters must be further scrutinized in order to develop an accurate equation, which can be used in engineering practice.

Moreover, scour countermeasures are used in order to reduce scour and protect the pier. The countermeasures are categorized as one of two types: flow-altering and armoring countermeasures. Different accessories are strategically placed upstream of the main pier in order to reduce the strength of the flow field and deflect the approach flow for the flow-altering countermeasures. Sacrificial piles, vanes, and collars are examples of flow-altering countermeasures (Tafarajnoruz et al., 2012). On the other hand, the flow-armoring countermeasures consist of a physical barrier placed around the base of the pier to increase the resistance of the bed material against the scouring process and reduce the scour depth around the pier. Riprap protection, cable-tied blocks, and Gabion mattresses are examples of flow-armoring countermeasures (Lagasse et al., 2007).

1.2. Objectives

This research will further investigate the effects of pier shape, the L/a ratio, and the efficiency of sacrificial piles on scour depth reduction. The objectives of this thesis are:

- Analyze the pier nose shape effect on scour geometry using round-nosed, sharp-nosed, and round-edged piers.
- Investigate the pier aspect ratio effect on scour depth.
- Explore the scour reduction by groups of five and three sacrificial piles in a triangular arrangement.
- Develop a scour prediction method using the results of the present investigation as well as literature.

1.3. Outline of the Thesis

The thesis is organized into five chapters:

Chapter 1 is dedicated to introducing the problem and outlining the problem statement. The literature review of parameters affecting scour, studies performed on scour around elongated piers and the effects of pier nose shape, and investigations of sacrificial pile arrangement and scour reduction are provided in Chapter 2. The methodology and experimental setup are presented in Chapter 3. An analysis of the results is shown in Chapter 4. Conclusions and recommendations for future investigations are included in Chapter 5.



Figure 1.1: Scour-related bridge failure in Alberta, Canada (CTV News, 2013)

CHAPTER 2

LITERATURE REVIEW

2.1. General Remarks on Scour Process

Scour is a common phenomenon, which occurs when the water flow exceeding a certain critical velocity interacts with a bridge pier. Up-on interaction with the pier, the flow generates a horseshoe vortex in the upstream region of the pier near the sand bed. This vortex is the main scour-causing flow structure. The trailing vortices and the wake vortices are produced at the sides and in the downstream part of the pier, respectively (Ettema et al., 2011), which also influence the scour and sediment transport process.

The flow approaching the pier is assumed to be fully developed, turbulent, and two-dimensional, while it becomes three-dimensional close to the pier. Further, when the flow reaches the upstream face of the pier, the velocity reduces to zero on stagnation and creates a downflow. In addition, on the sides and in the downstream region of the pier, the flow velocity increases (Figliola and Beasley, 2011). Thus, the pressure decreases around the pier in the downstream region. It is at the pier sides that scouring starts as the fluid velocity exceeds the critical velocity needed to initiate scour. Then, the scour increases in the upstream direction until it reaches the upstream face of the pier and removes the sediment around it to create the scour hole (Guo, 2012), as shown in **Figure 2.1**.

Furthermore, there is the presence of the wake vortices which are formed as a result of flow separation around the pier. A surface roller also forms at the air-water interface. The tornado-like action of the wake vortices removes the sediment from the bed in an upward motion. However, the volume of sediment transported by the wake vortices is not significant compared to the quantity of sediment transported by the horseshoe vortex (Chiew, 1984).

As mentioned earlier, scour can be classified into two types; clear-water and live-bed conditions. A clear-water condition occurs when the bed is not in motion making the net transported sediment to be zero. In this case, the equilibrium scour depth, occurs when the sediment in the scour hole cannot be removed anymore. The equilibrium is reached when critical shear stress of the bed material at the bottom of the scour hole is equal to the shear stress caused by the horseshoe vortex. In the field, the equilibrium scour depth under the clear-water condition

takes many days and even weeks to be reached (Chiew, 1984). On the other hand, the live-bed condition occurs when the sediment is transported from upstream of the pier to the downstream region. Equilibrium is reached when the rate of the transported sediment into the scour hole is equal to the transported sediment from the scour hole (Guo, 2012).

2.2. Parameters Affecting Scour

Previous studies have investigated various parameters, which influence the maximum scour depth. Most scour prediction methods are derived using empirical methods. However, most of these formulae over-predict scour depth (Williams et al., 2016). The equilibrium scour depth depends on parameters which can be classified into four groups, which are fluid properties, pier geometry, sediment properties, and time.

$$d_{se} = f \left[\begin{array}{l} \text{Fluid properties } (\rho, \vartheta, U, h, g, \theta); \text{ Pier geometry } (a, L, Sh, K_{sh}, Al); \\ \text{Sediment properties } (d_{50}, \sigma_g, U_c, \rho_s); \text{ Time } (t) \end{array} \right] \quad [2.1]$$

In **Equation 2.1**, ρ is the fluid density, ϑ is the kinematic viscosity, respectively, U is the flow velocity, h is the water depth, the acceleration due to gravity is g , θ is the angle of attack for the fluid properties. Concerning the pier geometry, a is the transverse pier width or the diameter for a circular pier, L is the pier length, Sh is the pier shape, K_{sh} is the pier shape factor, and Al is a parameter describing the alignment of the pier with respect to the approach flow. Sediment properties are described by the median sediment diameter d_{50} , σ_g is the uniformity of particle size distribution, U_c is the critical velocity of bed material required to initiate grain motion, and ρ_s is the sediment density (Melville and Chiew, 1999).

Most scour depth estimation methods use non-dimensional variables (**Equation 2.2**). In most laboratory conditions, the equation is modified for use for a given pier shape when the flow Reynolds number (Re) is high, the Froude number (F_r) is subcritical, and the approach flow is aligned with the pier.

$$\frac{d_{se}}{a} = f \left[\frac{h}{a}, \frac{U}{U_c}, \frac{a}{d_{50}}, \frac{L}{a}, Sh, Re, F_r, \frac{t}{t^*} \right] \quad [2.2]$$

Melville and Coleman (2000) used the flow shallowness factor (h/a) to classify the flow field. They categorized the piers as narrow when $h/a > 1.4$ and the pier width or diameter affects scour depth, intermediate when $0.2 \leq h/a \leq 1.4$ and the scour depth depends on both pier width and water depth, and wide when $h/a < 0.2$ and the scour depth is dependent on water

depth only (Melville and Coleman, 2000). Furthermore, using the flow velocity ratio (U/U_c), the clear-water and the live-bed conditions can be distinguished. When $U/U_c < 1$, the clear-water condition is maintained and the upstream sediment bed will not be in motion. The live-bed condition occurs when $U/U_c > 1$, and the sediment will be transported by the flow in this condition (Melville and Coleman, 2000).

Some previous investigations have focused on the relative coarseness (a/d_{50}) parameter. For instance, Melville and Coleman (2000) found that the influence of sediment is negligible when $a/d_{50} > 50$. In addition, Lee and Strum (2009) showed that when $a/d_{50} > 100$, the relative coarseness has a limited effect on scour depth due to the scaling of the sediment size (D'Alessandro, 2013). For the sediment effect on scour depth, the geometric standard deviation of the sediment σ_g , which is representative of the non-uniformity of the bed sediment, affects scour. It is shown that the scour depth becomes smaller with the use of large-sized particles and with increasing the flow intensity, the sediment non-uniformity σ_g effect on scour depth becomes minor (Ettema et al., 2011).

Melville and Chiew (1999) showed that the equilibrium time scale (t^*) for clear-water scour depends on the flow intensity (U/U_c), flow shallowness (h/a), and sediment coarseness (a/d_{50}). Further, small-scale laboratory tests in clear-water conditions showed that scour depth is less than 50% of the equilibrium scour depth after 10-12 hours. In some cases, it is necessary to run the experiments for several days to reach the equilibrium scour depth since the equilibrium time scale is a function of the flow U/U_c . For instance, in most cases, the scour depth varies between 50% and 80% of the equilibrium scour depth after 10% of the equilibrium scour time (Melville and Chiew, 1999).

2.3. Pier Effects

2.3.1. Pier Width and Arrangement

Pier width is one of the major parameters that affect scour depth and geometry. The frequency of the vortex shedding and the wake vortices are directly linked with the pier width. Previous investigations tested the influence of the pier width on equilibrium scour depth while holding the rest of the test parameters constant. They showed an increase in scour depth when the pier diameter increases (Ettema et al., 2006).

Most of the previous scour laboratory experiments were carried out using one main pier. Furthermore, piers are usually regarded as isolated in the design process without considering the influence of the arrangement of the piers and the effect of the proximity. For instance, Beg (2010) recorded an increase in scour depth by 95% using two circular piers in a transverse arrangement compared to an isolated pier under the same conditions. The lateral pier spacing was equal to zero. In addition, when the spacing was equal to a , the scour depth decreased by 21% compared to the test with lateral spacing S_{mp} equal to zero. The scour still decreased until S_p became equal to $8a$ under the same conditions. At that distance, the spacing had no effect on scour depth (Beg, 2010).

2.3.2. Pier Shape

The pier shape (Sh) makes the estimation of the scour depth more complicated due to the change in the interactions between the approach flow and the pier. Further, the horseshoe vortex and the wake vortices depend on Sh . There are few investigations on pier shape and its effect on scour depth. In addition, there is a shortage of approach flow data for most of pier shapes that are not cylindrical. Moreover, pier-shape factors (e.g. K_I or K_{sh} from HEC-18 equation) are used for some simple piers, such as rectangular, round-nosed, and sharp-nosed piers. K_{sh} is defined by the difference in local scour between circular piers and other pier shapes. Different researchers have carried out investigations on pier shape factors, including Laursen and Toch (1956), Chabert and Engeldinger (1956), Venkatadri et al. (1965), and Ettema (1980). **Table 2.1** shows the different shape factors found in the studies cited above. However, those factors can only be used for specific pier shapes and in cases where the approach flow is aligned with the pier (Obeid and Al-Shukur, 2016).

Table 2.1: Pier shape factor K_{sh} values (Obeid and Al-Shukur, 2016)

Pier shape	K_{sh}
Circular	1
Rectangular	1.1
Rectangular round-nosed	1
Rectangular square-nosed	1.2
Oblong	0.85
Streamlined	0.48
Elliptical	0.8
Sharp nose	0.9

Tseng et al. (2000) carried out numerical simulations to compare the three-dimensional flow around circular and square shapes. It was found that the domains of the horseshoe and wake vortices were smaller for the circular pier than the square pier. In addition, the position of the horseshoe vortex was closer to the front face of the circular pier compared to the square pier. In the downstream region, it was shown that the strength of the wake vortices was greater for the square pier compared to the circular pier. Consequently, the equilibrium scour depth was bigger for the square pier compared to the circular pier.

A study by Obeid and Al-Shukur (2016) considered the effect of pier shape on scour depth and geometry. Three different flow intensities ($U/U_c = 0.56$, $U/U_c = 0.79$, and $U/U_c = 0.92$) were used with various pier shapes with $L/a = 4$ as shown in **Table 2.2**. In addition, the percentage of scour reduction or increase for a given pier shape compared to the circular pier is displayed in **Table 2.2**. For instance, the rectangular pier recorded an increase in scour depth by 10% for $U/U_c = 0.92$ against a reduction in scour depth by almost 19% for the elliptical pier, when both were compared to the circular pier under the same conditions. In addition, the streamline pier recorded the minimum scour depth for all three flow intensities used (Obeid and Al-Shukur, 2016). However, some of the pier shapes used in the investigation, such as joukowsky and octagonal have high cost and difficulty in construction.

Table 2.2: Measured scour depth of different pier shapes with three different flow velocities
(Obeid and Al-Shukur, 2016)

Pier Shape	$U/U_c = 0.56$	$U/U_c = 0.79$	$U/U_c = 0.92$
	Scour reduction*	Scour reduction*	Scour reduction*
Circular	-	-	-
Rectangular	+10.26%	+11.48%	+ 10.14%
Oblong	+5.13%	-24.59%	-15.94%
Elliptical	-7.69%	-19.67%	-18.84%
Chamfered	+5.13%	-3.28%	-2.90%
Octagonal	+7.69%	-14.75%	-14.49%
Sharp nose	-23.08%	-26.23%	-28.99%
Hexagonal	-28.21%	-40.98%	-40.58%
Streamline	-51.28%	-57.38%	-56.52%
Joukowsky	+20.51%	-9.84%	-11.59%

*Scour reduction as compared with circular cylinder.

2.3.3. Elongated Pier

As previously mentioned, many studies used circular piers and piers with simple shapes to investigate the scour depth and the approach flow. In practice, elongated piers are commonly used in the design of bridge piers. However, few experimental studies have investigated this type of geometry.

Debnath and Chaudhuri (2012) investigated the scour around elongated piers in a clay-sand mixed cohesive bed with $d_{50} = 0.18$ mm. The piers were circular, square with $L/a = 1$, and rectangular and round-nosed piers with $L/a = 2$. The scour depth was 15% lesser for the round-nosed pier when compared with the circular pier, while the rectangular and square piers had a much a scour increase of 41% and 11% than the circular pier, respectively. The scour hole for the square pier was relatively larger when compared with the other piers due to the strength of the horseshoe vortex upstream of the pier, the downflow, and the highest bed shear stress. ADV

measurements were carried out at 60 mm upstream from the pier in this study. Close to the bed, it was observed that the Reynolds shear stress profiles were similar for all the piers. However, the magnitude of the near-bed Reynolds shear stress at the side of the pier was minimum for the round-nosed pier and maximum for the square pier. As a result, the equilibrium scour depth was almost 50% lesser for the round-nosed pier when compared with the square pier.

Lima (2014) studied the flow characteristics around a round-nosed pier with $L/a = 2$ using two-component LDV measurements. It was observed that upstream of the pier, the streamwise velocity U was slightly lower than the test in the absence of the pier. Further, the approach flow decelerated and deflected towards the bottom.

Another investigation was carried out by Azevedo et al. (2014) in which circular and round-nosed ($L/a = 2$) piers were used. The scour depth for the round-nosed pier decreased by 9.5% compared to the circular pier. Further, the equilibrium scour for the elongated pier was reached earlier than the circular pier. This was due to the flow contraction around the elongated pier, which secluded the horseshoe vortex inside the scour hole. In addition, the interaction between the approach flow and the pier nose in the upstream region made the sediment erosion more difficult. Therefore, the scour depth was less for the round-nosed pier.

Vijayasree et al. (2017) investigated the approach flow using a ADV and studied the local scour around pier of different shapes. The pier shapes were rectangular, oblong, trapezoidal, triangular, and lenticular with $L/a = 5$. The rectangular pier had the maximum scour depth with scour increase of 30% when compared with round-nosed pier. However, the triangular and lenticular piers recorded the minimum d_{se}/a with scour reduction of 24% and 50%, respectively. This was due to the immediate bifurcation of the horseshoe vortex close to the lenticular and triangular piers. It was observed from the ADV data that near the bed, the streamwise velocity magnitude for the rectangular, oblong, and trapezoidal piers were prominent at the upstream and the downstream regions. However, the horseshoe vortex circulations were not that significant for the triangular and lenticular piers. This was due to the frontal scour position generated by the horseshoe vortex. The frontal scour for the sharp-nosed piers is generated at the leading edges. However, the scour generation occurred at the center of the rectangular, oblong, and trapezoidal piers.

Roy (2017) carried out experiments for different pier shapes (circular, rectangular, and oblong piers) with $L/a = 2$. The clear water condition was maintained at three flow velocities. A

uniform coarse sediment bed was used with $d_{50} = 0.95$ mm for all the tests. It was found that the scour depth decreased drastically with the change of pier geometry and increased with the increase of the flow velocity for all the tests. The rectangular pier had the maximum scour depth, while the oblong pier had the minimum scour depth. An increase in the scour depth occurred with an increase in the intensity of flow parameters and vice versa. More importantly, it was reported that the equilibrium scour depth was directly dependent on the exposed open face of the pier nose in contact with the approaching flow. As a result, the oblong pier had the minimum scour depth and recorded a 50% reduction in scour depth compared to the rectangular pier.

The downstream geometry of scour is also affected by pier geometry. Chavan et al. (2018) studied the scour depth around a circular pier with a diameter $a = 75$ mm and two oblong piers with $L/a = 3$ and 3.6, respectively. They reported that the circular pier had a larger scour depth than the two elongated piers. The scour depth around the oblong piers was around 15% less compared to the circular pier under the same experimental conditions. Further, for the scour hole, the deposition of the height and length at the downstream region of the pier was larger for the circular pier compared to the oblong piers.

Most of the elongated pier investigations have been carried out using round-nosed, sharp-nosed, rectangular, and triangular piers. The round-nosed and the sharp-nosed piers have recorded a scour depth reduction compared to the circular pier in most of the investigations cited above. However, the rectangular piers had the largest scour depth in all the investigations that used this pier shape. Moreover, some studies investigated the changes in approach flow around the elongated piers using ADV measurements, such as Debnath and Chaudhuri (2012) and Vijayasree (2017).

2.4. Bridge Pier Countermeasures

Local scour countermeasures are a commonly used to protect bridge piers against the scour process. There are different scour countermeasure methods, which can be classified into two categories: flow-altering countermeasures and bed-armoring countermeasures. The flow-altering countermeasures are implemented to decrease the strength of the horseshoe vortex and the downflow by diverting the approach flow, such as sacrificial piles, collars, submerged vanes, and pier slots. Bed-armoring countermeasures provide physical barriers to protect erodible bed material, include riprap, cable-tied blocks, and gabions. (Melville and Hadfield, 1999).

2.4.1. Efficiency of Countermeasures

The efficiency of the countermeasure against scour is defined by the scour reduction

Equation 2.3. Here, r_{de} is a function of the equilibrium scour depth around the unprotected and protected piers.

$$r_{de}(\%) = \frac{d_{se0} - d_{se}}{d_{se0}} \times 100 \quad [2.3]$$

In **Equation 2.3** d_{se0} and d_{se} are the equilibrium maximum scour depth for the unprotected and the protected pier, respectively. The location of the maximum scour depth depends on the countermeasure method and the set-up used in the experiments (Tafarojnoruz et al., 2012).

2.4.2. Use of Collars

Collars are thin horizontal plates placed around the bridge pier. The collar can protect the pier against scour by deflecting the downflow and reducing the horseshoe vortex, thereby reducing the scour around the main pier.

The scour reduction using collars depends on the size and location of the collar. However, even a large collar may not completely eliminate scour. Further, it creates other sediment-related problems at the boundary of the collar (e.g. uplifting due to migration under live-bed conditions). The collar can be placed below the undisturbed bed level, above or just in a horizontal position. **Figure 2.2** shows the collar countermeasure method where h_c is the distance between the collar and the surface of the water, and w_c represents the collar width (Melville et al., 1998).

Kayaturk et al. (2004) studied the effect of the collars at the abutment at different elevations and various sizes. A decrease by 67% in scour depth resulted when the collar was placed at a height of 50 mm below the bed. Moreover, Masjedi et al. (2010) investigated the collar widths effect on scour depth. The collars were placed around an oblong pier at the bed level. A maximum scour reduction by 78% was achieved when the collar width was equal to $3a$ (a is the width of the pier) and $\frac{w_c}{a} = 3$. Although these and many other investigations have indicated that the use of collars may significantly reduce the depth of scour, collar installation in the field is viewed as impractical due high overhead for construction and other environmental factors which may influence collar stability and performance (Lagasse et al., 2007).

2.4.3. Sacrificial Piles

Sacrificial piles are a type of flow-altering countermeasure placed upstream of a main pier to deflect the approach flow velocity, reduce velocity in the wake region of the sacrificial piles, and reduce the horseshoe vortex at the upstream of the main pier. As a result, erosive potential is minimized in the region between the sacrificial piles and the main pier. Different parameters affect the efficiency of this method, including the number of piles (N_p), pile characteristics (pile diameter D_p , shape, etc.), the distance between the sacrificial piles and the pier (X_p), their arrangement, and the protrusion of each pile (fully or partly submerged) (Melville et al., 1998).

The arrangement of the piles is a significant factor in the efficacy of this method. One or numerous piles can be placed upstream of the main pier. For instance, a triangular array with an apex of the triangle pointing upstream has been tested in the previous experiments and has been found to be one of the best configurations in terms of scour depth reduction (Melville et al., 1998).

Several investigations have been carried out by different researchers using different numbers and arrangements of piles. An early study by Chabert and Engeldinger (1956) gave a 50% reduction in scour depth using a triangular pattern. No further details were provided about the investigation. Shen et al. (1966) recorded a 66% reduction in scour depth with the use of one pile placed at a distance $X_p = 2a$ from the main pier. Further, different arrangements of three sacrificial piles were investigated by Karim and Chang (1972). The triangular arrangement recorded a decrease by 65% in scour depth while a 60% reduction was reported when the three piles were aligned at $X_p = 2a$ from the main pier.

Paice and Hey (1993) carried out an investigation utilizing four sacrificial piles in a diamond-shaped configuration. The scour depth decreased by around 63% compared to the test without countermeasures. Another study by Melville and Hadfield (1999) investigated the efficiency of the different pile positions and the various geometric parameters. The wedge of pile group angle α , the horizontal spacing between the sacrificial piles S_p and the distance between the sacrificial piles and the main pier X_p were tested in this study. The authors observed a reduction of 56% for a circular pier and a decrease by more than 30% for the rectangular pier using five sacrificial piles in a triangular arrangement when $\alpha = 30^\circ$, $S_p = 0.67a$, and $X_p = 2a$. Similar to Melville and Hadfield (1999), Parker et al. (1998) used five sacrificial piles placed in a triangular

array with $\alpha = 30^\circ$, $S_p = a$, and $X_p = 2.5a$. They recorded a decrease by 41% in the scour depth. Furthermore, a reduction of 50% in scour depth was recorded by Haque et al. (2007) using three side-by-side sacrificial piles located at a distance equal to $2b_p$ (b_p is the projected width of the pier) upstream of a rectangular pier.

Transverse and tandem arrangements of sacrificial piles have also been explored experimentally in literature. In an investigation by Tafarojnoruz et al. (2012), scour reduction using sacrificial piles was investigated for two circular piers of diameters $a = 40$ and 48 mm, respectively. A maximum reduction of 32.5% recorded with the use of three sacrificial piles in a transverse arrangement and placed at a distance $X_p = 2a$, as shown in **Figure 2.3**. Further, Wang et al. (2016) recorded 21% in scour depth using a single pile. In addition, a decrease by 35% was recorded when one sacrificial pile was utilized with the two main circular piers placed in a tandem arrangement. More recently, Fouli and Shabayek (2017) observed a reduction of 52% using one sacrificial pile placed at a distance $X_p = 1.5a$.

The use of sacrificial piles has also been occasionally investigated under field conditions. A field study was also carried out by Karim and Chang (1972) on a bridge over the Big Sioux River in South Dakota, USA. Three sacrificial piles in a triangular array were installed in front of three pairs of circular piers. They resulted in a reduction in scour depth of 44%. Chang and Karim (1972) also concluded that the effect of sacrificial piles was related to the deviations in the direction of the flow and that the scour depth could be reduced or even eliminated in some cases. Change in approach flow angle can occur due to several factors, such as long-term changes in the direction of the river due to the modification in flow direction upstream. Paice et al. (1993) installed pile groups at three different locations on the Severn River, UK, with no significant floods happened during the period of the investigations. Preliminary data showed that the installed piles reduced the scour in all three bridges. No further details were given about the study.

Most of the previous investigations using sacrificial piles have been conducted on a circular pier. Only two studies were carried out using rectangular piers. An investigation into the best sacrificial piles configuration was conducted by Karim and Chang (1972) and recorded a 65% decrease in scour depth for a circular pier and more than 30% decrease in scour depth for a rectangular pier using three sacrificial piles in a triangular arrangement. A decrease by 60% resulted by Paice et al. (1993) in scour depth using diamond shape arrangement. Melville and

Hadfield (1999) noted a 56% decrease in scour depth using five sacrificial piles in a triangular array. Most of the investigations used different parameters, such as the number of sacrificial piles, X_p , S_p , pile arrangements, and configurations, in order to observe the best configuration to reduce scour depth. To date, no investigation have combined the effects of pier nose shapes, L/a ratio, and sacrificial piles for optimal scour depth reduction.

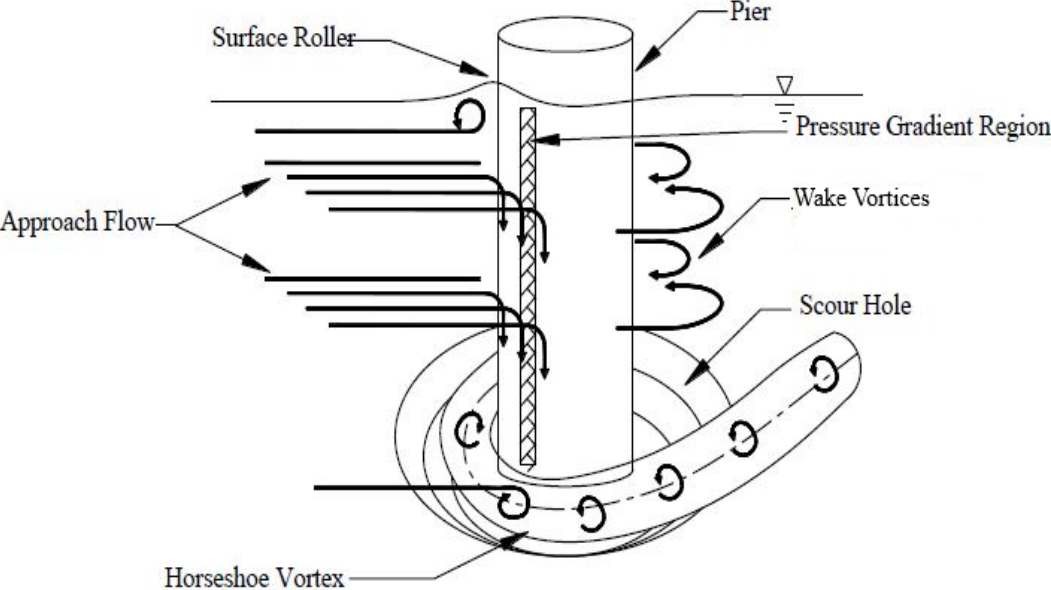


Figure 2.1: Description of flow structures around a pier (Hodi, 2009)

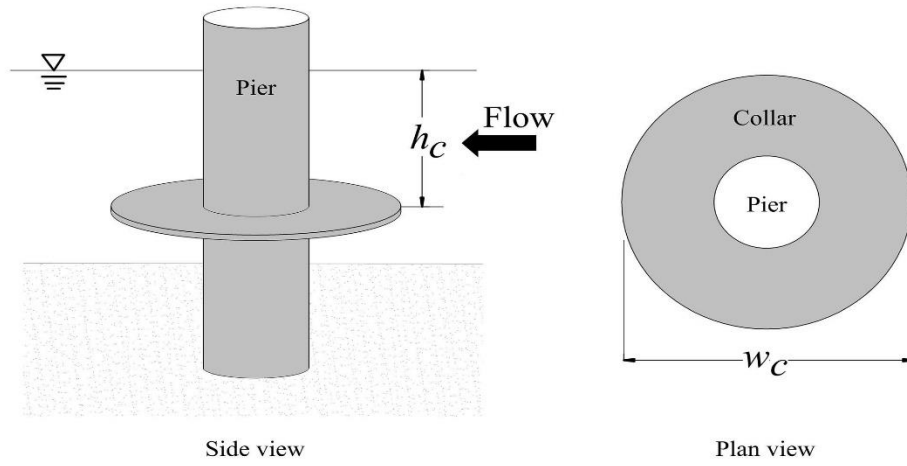


Figure 2.2: Collar (Plan and side views)

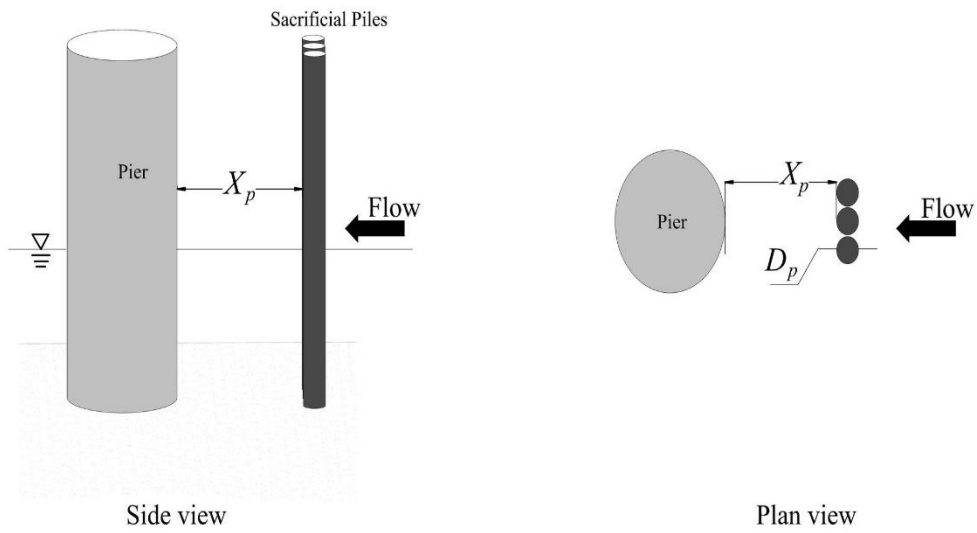


Figure 2.3: Schematic of the sacrificial piles in a transverse arrangement

CHAPTER 3

METHODOLOGY

3.1. Experimental Set-Up

The experiments were conducted in the Sedimentation and Scour laboratory located in the Ed Lumley Center for Engineering Innovation at the University of Windsor, Ontario, Canada. The laboratory contains a horizontal flume 10.5 m in length, 1.22 m in width, and a height of 0.84 m. **Figure 3.1** shows a schematic of the flume.

The flow progression on to the sediment bed takes place by an approach ramp. All the tests were under the clear water conditions with flow intensity $U/U_c = 0.9$. Flow in the flume was calibrated using a V-notch weir located at the downstream end of the flume. Two flow straighteners were located upstream of the bed in order to decrease the turbulence levels. A boundary layer trip was installed at the upstream boundary of the sand bed. An additional 3 mm diameter trip rod was placed on the sand bed at a distance of 0.5 m from the boundary layer trip to ensure fully developed flow at the measurement location. **Figure 3.2** shows the streamwise velocity at $X = 3.5\text{m}$ in the absence of the pier in the presence and in the absence of the 3 mm trip rod. The setup been used in other scour studies and flow quality has been ensured by many researchers using the same facilities (Williams et al. (2016 and 2018), and Wu et al. (2016)).

3.2. Bed Material

An ASTM sieve analysis was performed for the sediment used in the experiments to determine the grain size distribution and characteristics (**Figure 3.3**). The bed material used was classified as fine sand with $d_{50} = 0.74$ mm. The standard deviation of particle size ($\sigma_g = \sqrt{d_{84}/d_{16}}$) was equal to 1.48. The sediment was further classified as poorly graded and uniformly distributed. The critical velocity (U_c) was resolved using the experimental and analytical methods and was found to be equal to 0.306 m/s.

3.3. Experimental Procedures

Each experiment was carried out for 24 hours. Melville and Chiew (1999) showed that the equilibrium scour depth varied between 50% and 80% during the first 10% of the equilibrium

scour time. Further, after 24 hours, the scour depth reached 80% to 90% of the equilibrium scour depth. D'Alessandro (2013) demonstrated that between 12 and 24 hours, an asymptotic state in scour depth is reached and that the scour width after 24 hours did not increase. In addition, Kharbeche et al. (2021) observed a significant change in scour depth between the first and second hour of testing. In addition, more than 90% of the equilibrium scour depth was attained after 24 hours. Therefore, 24 hours was considered to be an acceptable time length for this study.

For the scour experiments, before running a given test, the sand was leveled using a flat trowel and a water level meter. The pier (pier width $a = 51$ mm for all the tests) was placed at the centerline position and at a distance $X = 3.5$ m from the boundary layer trip. For Series A, varying pier shapes with $L/a = 1, 2,$ and 4 were tested. In Series B and Series C, five and three sacrificial piles were placed upstream of the main pier at a distance $X_p = 2a$. The origin of the scour graphs (to be displayed in **Section 4**) was the center of the pier with $X = 3.5$ m from the boundary layer trip, Y was at the centerline of the flume, and Z was at the bed level. After leveling the sand bed and installing the required piers, the flume was filled with the desired water depth ($h = 0.12$ m). The pump was turned on and the frequency was increased gradually until it reached 16 Hz in order to achieve a flow intensity $U/U_c = 0.9$.

After running a given test for 24 hours as indicated above, the pump frequency was brought down gradually and then shut off. To avoid the sediment displacement in the scour formation, the water was drained slowly through the settling tank and outlet tank drains. The contour profile and the scour hole were carefully identified and a Leica Laser Distance Meter (LDM) was used to measure the centerline and contour profiles. **Figure 3.4** shows the centerline profile of a typical scour test.

3.4. Flow Measurements

Laser Doppler Velocimeter (LDV) measurements were taken in the absence of the pier at the flume centerline ($Y = 0$) at a streamwise position equal to 3.5 m downstream of the beginning of the sediment recess, as shown in **Figure 3.5**. The LDV system is an optical measuring technique used to determine the velocity of a fluid with high temporal resolution. The flow velocity measurements are taken at one point. The flow was seeded with particles since the LDV uses the Doppler technique to calculate the velocity of particles in the fluids. LDV measurements were taken after the flow was run for two hours, and 20000 samples were acquired at each measuring

point. The velocity span was equal to 0.74 m/s, sensitivity of the laser was equal to 1400 V and the gain was equal to 24 dB in order to attain a sufficient data signal to collect the data. A Burst Signal Processor (BSA 3) from Dantec Dynamics was used for the signal processing.

A downward looking Acoustic Doppler Velocimeter (ADV) measurements were also taken in the absence of the pier. The ADV was placed at a distance $X = 3.5$ m from the boundary layer trip at $Y = 0$ in order to capture the approach flow characteristics, as shown in **Figure 3.5**. The ADV system also uses the principle of Doppler shift, and more specifically, the pulse-to-pulse coherent technique. This technique transmits a series of short sound pulses, measures the alteration in the pitch and of the returned sound after receiving their echoes. It measures the flow velocity and record the instantaneous velocity components in the three directions (Chanson et al., 2005). It should be noted that ADV measurement cannot be acquired near the free surface due to the limitations of the system. All the ADV measurements were acquired two hours after starting a given scour test. The frequency of data acquisition was equal to 100 Hz, with a 5 minutes sampling duration, and a velocity range = ± 30 cm/s. The data collection was equal to 3000 samples. The data was filtered by removing low correlation threshold ($< 75\%$), and low signal-to-noise ratio (SNR < 20 dB). **Figure 3.6** shows the sand bed with the main pier, sacrificial piles, and the location where the ADV measurements were taken.

ADV measurements were also taken around the piers for 6 out of the 12 tests with sacrificial piles at $Y = 0$ at a location 0.2 m upstream of the sacrificial piles. The tests were B6, B7, and B8 using five sacrificial piles, and C8, C9, and C10 with three sacrificial piles to study the effect of the sacrificial piles on the characteristics of the approach flow. The test series are described in the next section. Furthermore, ADV measurements were acquired at the side of the pier in order to obtain the separation velocity profiles for the square pier with $L/a = 1$ and the round-nosed, sharp-nosed, and round-edged piers with $L/a = 4$. The ADV was placed along the midpoint between the center of the pier and the sidewall at the position $X = 3.5$ m from the boundary layer trip, $Y = -b/4$ m from the centerline, and at a depth of $Z = 0.35$ m, as shown in **Figure 3.7**.

3.5. Experimental Program

Experiments were divided into three series of tests. Series A was carried out for different pier shapes and various L/a ratios. The pier shapes with various L/a ratios used for Series A are shown in **Figure 3.8**. Series A investigated the effect of pier shape and L/a ratio on scour depth. The shapes were circular, diamond, round-edged, and square with $L/a = 1$, and round-nosed,

sharp-nosed, and round-edged piers with $L/a = 2$ and 4, respectively. The width of all the piers was $a = 51$ mm.

In Series B, five sacrificial piles were used in a triangular shape to study the impact of the sacrificial piles on scour geometry, including the scour depth reduction. The piers shapes used in Series B were round-nosed, sharp-nosed, and round-edged piers with $L/a = 2$ and 4, respectively. The sacrificial pile diameter D_p was equal to 10 mm, the distance between the main pier and the sacrificial piles X_p was equal to $2a$, the distance between two sacrificial piles S_p was equal to $0.67a$, and the wedge of pile group angle α was equal to 30° . The same arrangement was conducted by Melville and Hadfield (1999), where a 56% reduction in scour depth was observed for a circular pier. **Figure 3.9** shows the five sacrificial piles in a triangular arrangement.

Experiments with three sacrificial piles were conducted in Series C. In Series C, D_p was equal to 10 mm, X_p was equal to $2a$, and S_p was equal to a , as displayed in **Figure 3.10**. The same arrangement was used by Chang and Karim (1972) and a reduction of 65% was recorded.

In all the tests, the non-dimensional parameters were held constant. The flow intensity U/U_c was held to 0.9 to maintain a clear water condition, the flow shallowness h/a was 2.4 to ensure that the piers were classified as narrow, the blockage ratio a/b was 4.2% to minimize the effects of secondary currents and the relative coarseness a/d_{50} was 66 to minimize sediment scaling effect. The Froude number was equal to 0.26 and the Reynolds number was equal to 13209 in all the experiments, as shown in **Table 3.1** in order to ensure that flow was subcritical and turbulent. The experimental program is shown in **Table 3.2**. $h = 0.12$ m and the flow velocity $U = 0.28$ m/s for all experiments.

Table 3.1. Dimensionless parameters in all the experiments

U/U_c	h/a	a/b	a/d_{50}	F_r	Re
0.9	2.4	4.2%	66	0.26	13209

Table 3.2: Experimental program

Test ID	Pier shape	a (mm)	L (mm)	L/a	N_p	S_p (mm)	α
A1	Circular	51	51	1	-	-	-
A2	Diamond	51	51	1	-	-	-
A3	Round edges	51	51	1	-	-	-
A4	Square	51	51	1	-	-	-
A5	Round nose	51	102	2	-	-	-
A6	Sharp nose	51	102	2	-	-	-
A7	Round edges	51	102	2	-	-	-
A8	Round nose	51	204	4	-	-	-
A9	Sharp nose	51	204	4	-	-	-
A10	Round edges	51	204	4	-	-	-
B5	Round nose	51	102	2	5	34	30°
B6	Sharp nose	51	102	2	5	34	30°
B7	Round edges	51	102	2	5	34	30°
B8	Round nose	51	204	4	5	34	30°
B9	Sharp nose	51	204	4	5	34	30°
B10	Round edges	51	204	4	5	34	30°
C5	Round nose	51	102	2	3	51	30°
C6	Sharp nose	51	102	2	3	51	30°
C7	Round edges	51	102	2	3	51	30°
C8	Round nose	51	204	4	3	51	30°
C9	Sharp nose	51	204	4	3	51	30°
C10	Round edges	51	204	4	3	51	30°

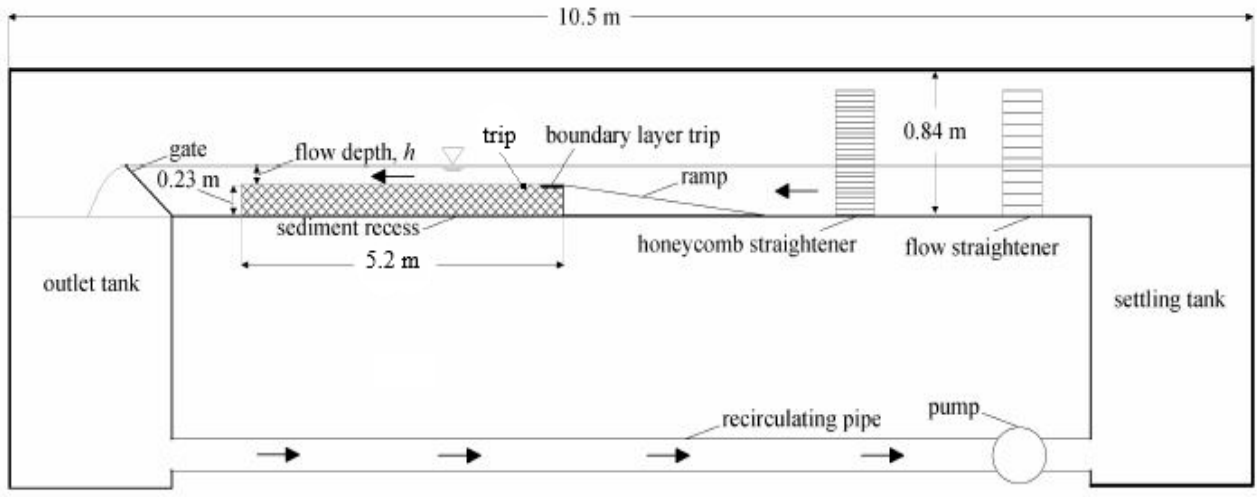


Figure 3.1: Schematic of the horizontal laboratory flume used for the experiments (modified from (Williams, 2019))

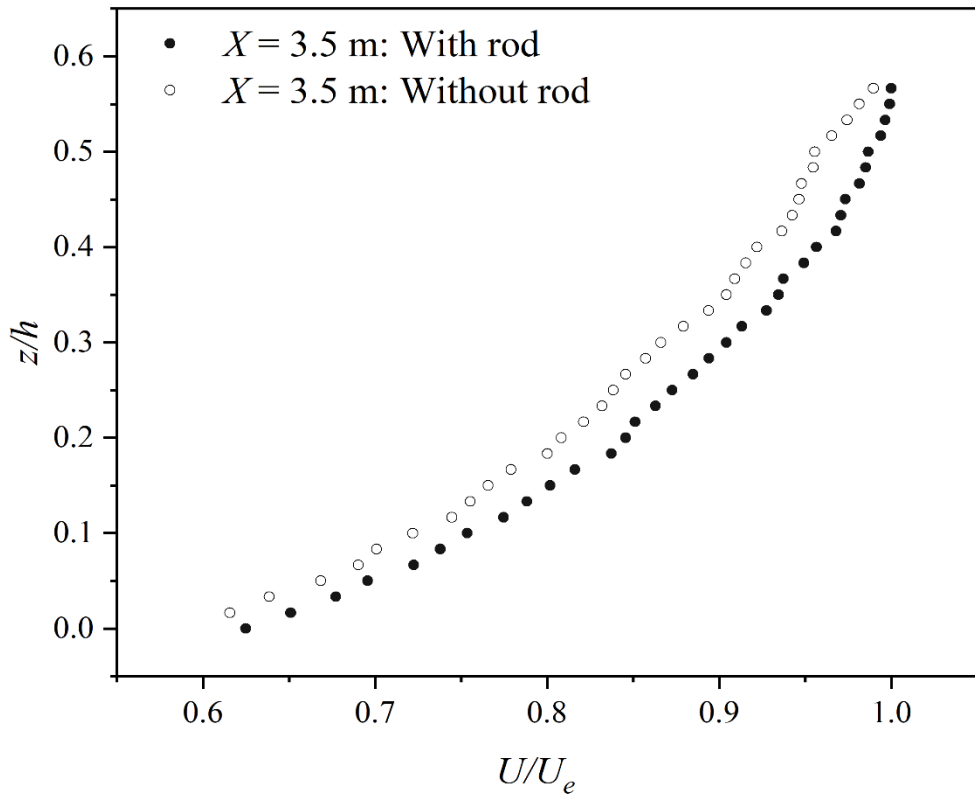


Figure 3.2: Streamwise velocity profiles in the presence and in the absence of the 3 mm rod placed in the sand bed

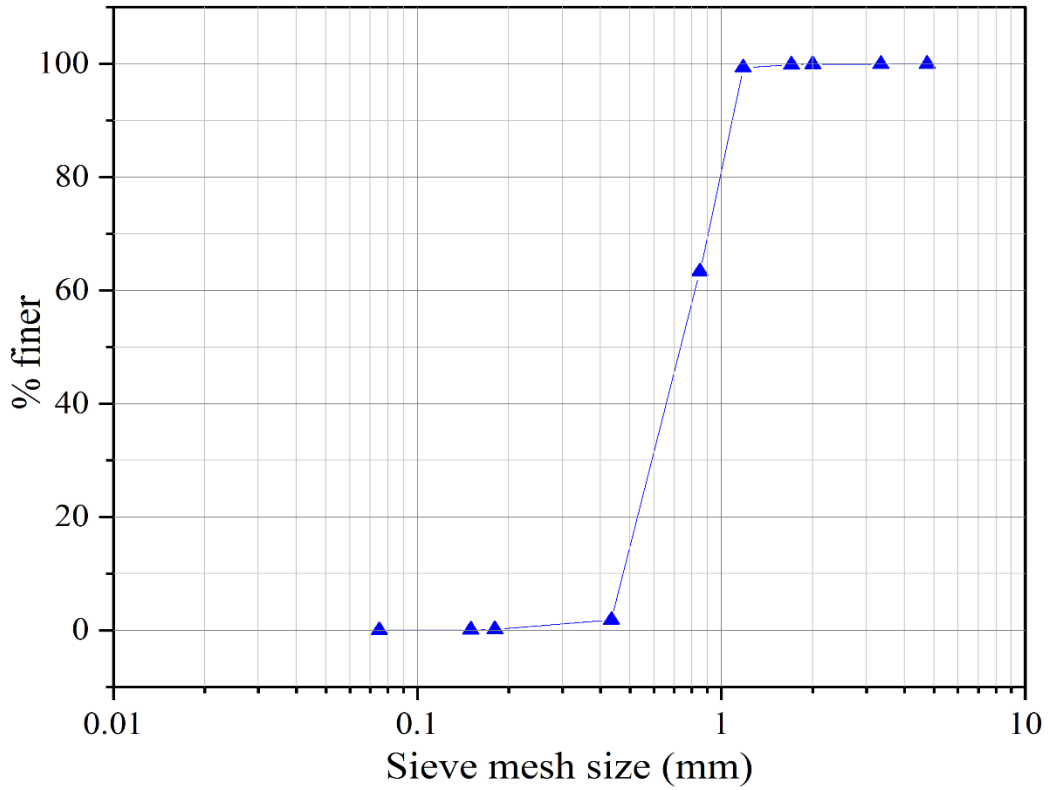


Figure 3.3: ASTM sieve analysis for bed sediment used in the experiments

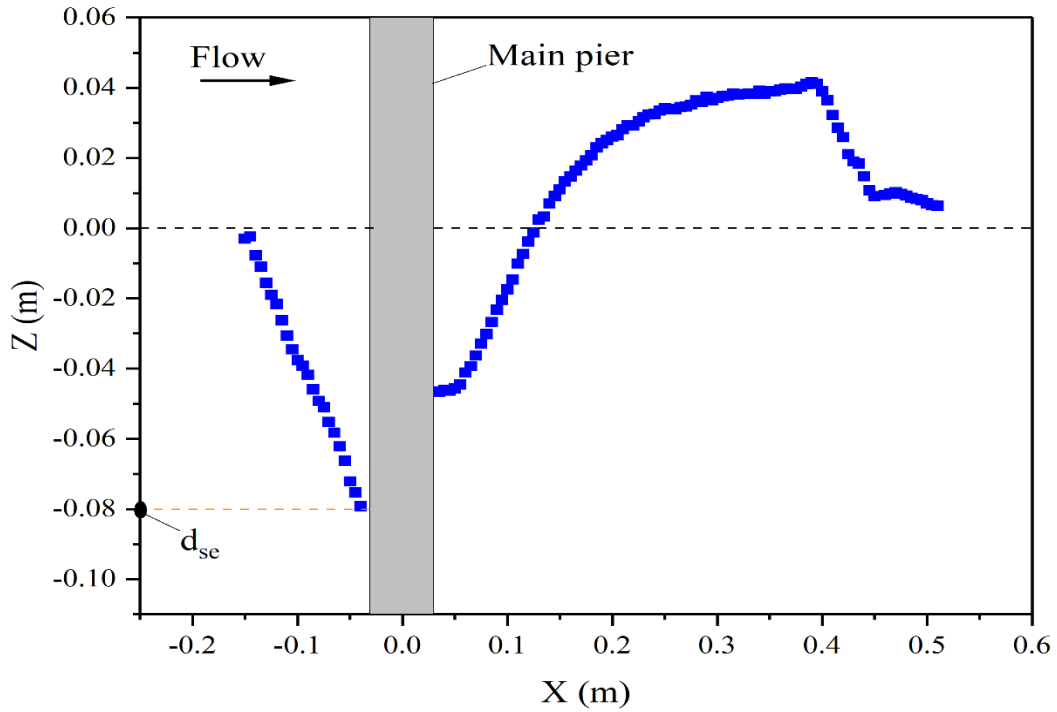


Figure 3.4: Point measurements of a typical scour hole centerline profile

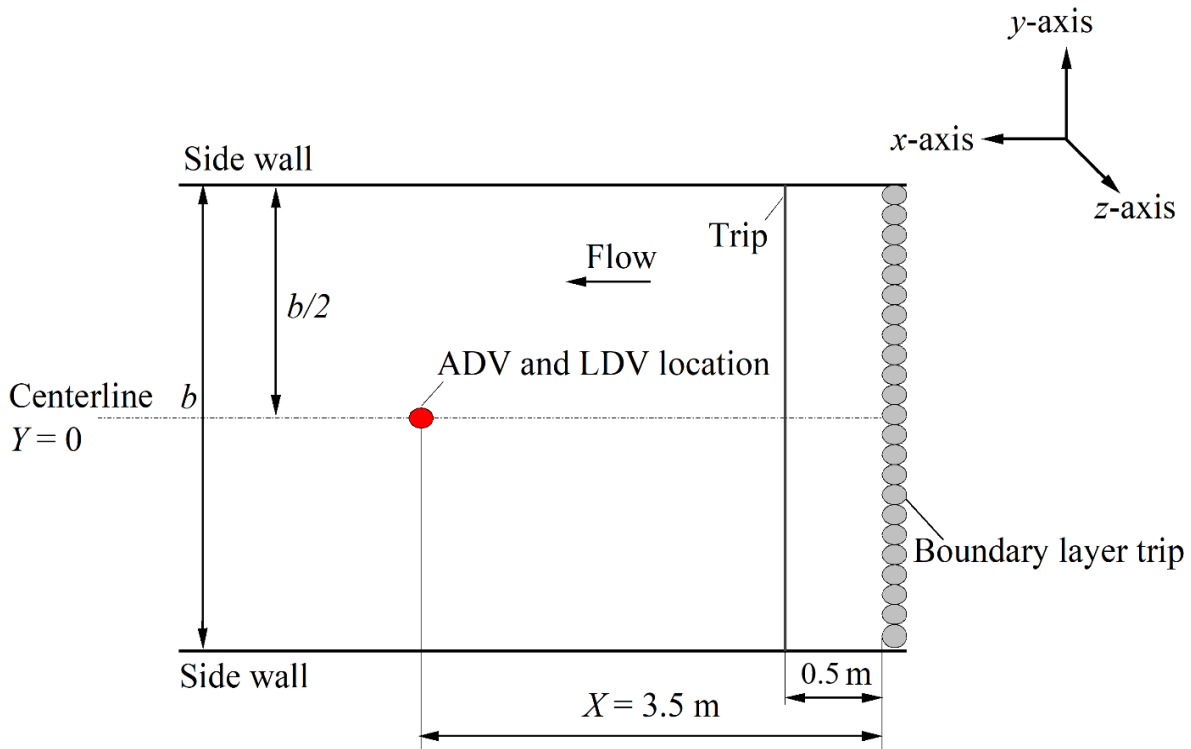


Figure 3.5: Location of the ADV and LDV for the tests in the absence of the pier

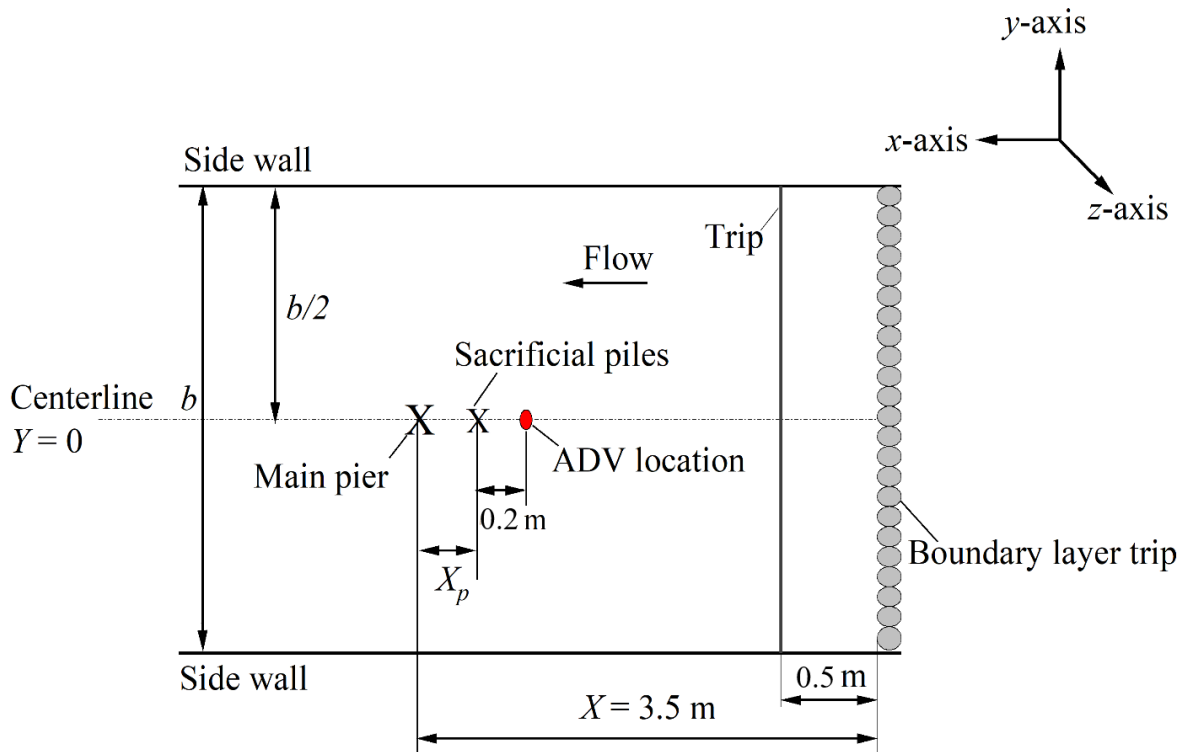


Figure 3.6: Location of the ADV for tests with 5 and 3 sacrificial piles (B6, B7, B8, C8, C9, and C10)

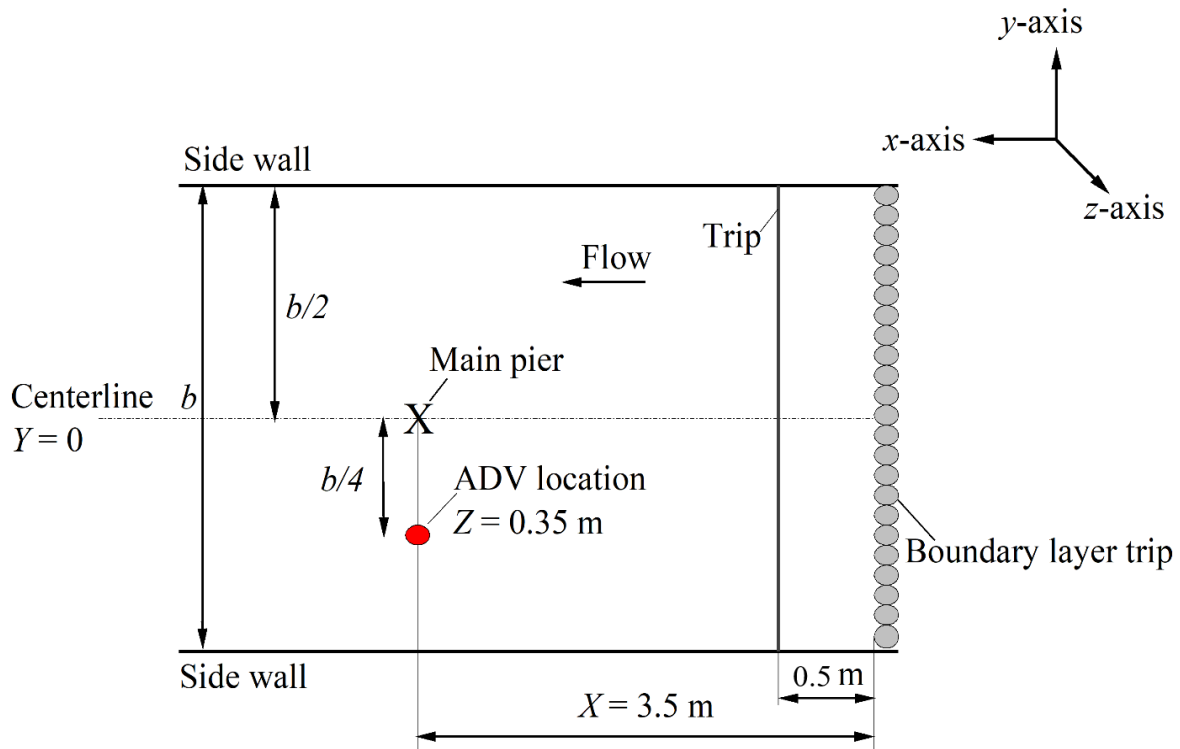
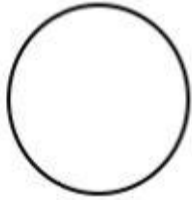
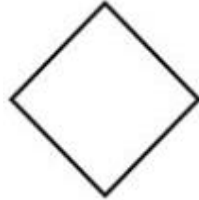


Figure 3.7: Location of the ADV for the tests (A4, A8, A9, and A10) to get the separation velocity

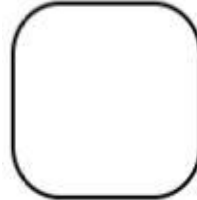
$L/a = 1$



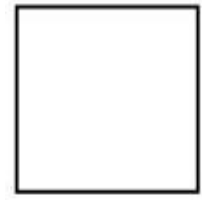
A1: Circular



A2: Diamond



A3: Square with round edges

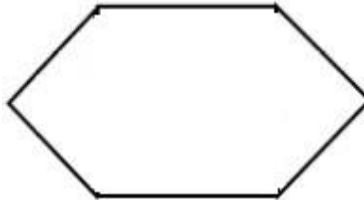


A4: Square

$L/a = 2$



A5: Round nose



A6: Sharp nose



A7: Round edges

$L/a = 4$



A8: Round nose



A9: Sharp nose



A10: Round edges

Figure 3.8: Different pier shapes and L/a ratios

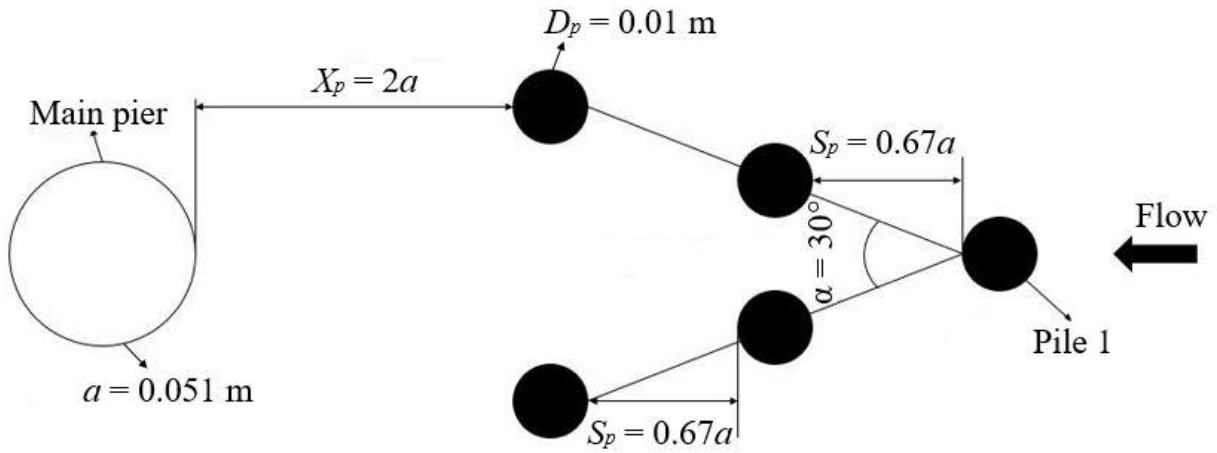


Figure 3.9: Schematic of the five sacrificial piles used in Series B

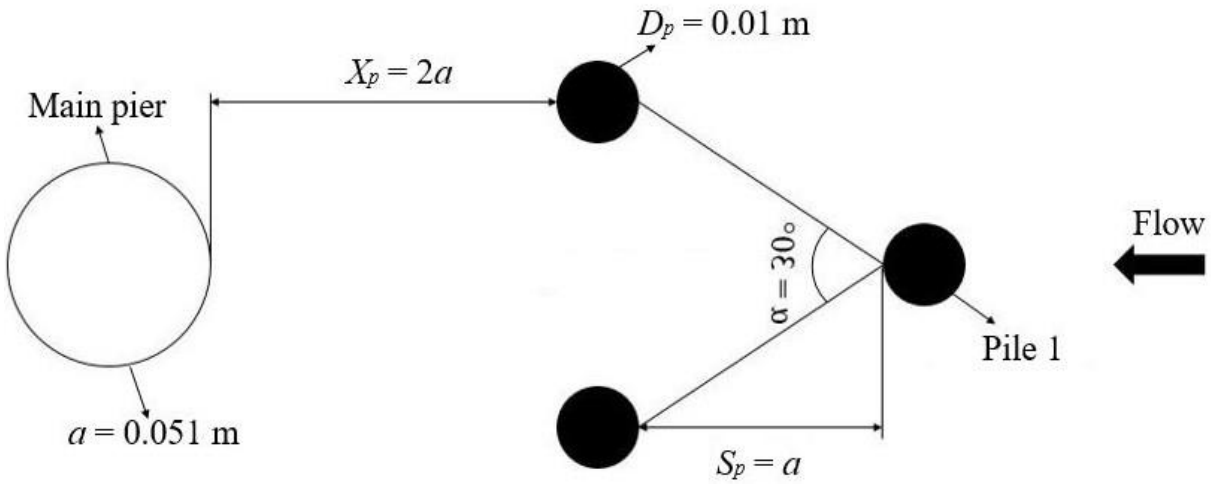


Figure 3.10: Schematic of the three sacrificial piles used in Series C

CHAPTER 4

RESULTS AND DISCUSSION

This chapter is composed of two main sections: the first part deals with the approach flow, while the subsequent section will discuss the results of the scour experiments. In terms of scour analysis, Series A studies the effect of pier shape and aspect ratio (L/a) on scour depth. Series B and Series C investigate the impact of sacrificial piles on scour, and the scour depth reduction using five and three sacrificial piles in a triangular arrangement, respectively.

4.1. Approach Flow Analysis

The approach flow conditions for various tests are shown in terms of the normalised mean streamwise velocity profiles (**Figures 4.1** and **4.2**) and normalized Reynolds shear stress profiles (**Figures 4.3**, and **4.4**). Tests E and L represent the experiments carried out in the absence of the pier at $X = 3.5$ m and at the centerline location using the ADV and the LDV, respectively. The ADV and LDV locations to measure the approach flow in the absence of the pier are shown in **Figures 3.5**. The streamwise velocity and the Reynolds shear stress quantities were normalized by the maximum velocity $U_e = 0.28$ m/s obtained from the LDV test in the absence of the pier. It should be noted that ADV measurements are not possible near the free surface. **Figure 4.1** outlines the streamwise velocity profiles for three tests bearing five sacrificial piles compared to tests E and L. The three experiments are comprised of tests B6 and B7 with $L/a = 2$, and B8 with $L/a = 4$. The normalized streamwise velocity profiles (U/U_e) for tests C8, C9, and C10 with $L/a = 4$ are shown in **Figure 4.2**. The results also compared the corresponding U/U_e profiles to tests E and L in the absence of the pier. The ADV location to measure the approach flow upstream of the sacrificial piles is shown in **Figures 3.6**.

The results outlined in **Figures 4.1** and **4.2** show that U/U_e for Series B and Series C tests are similar to the approach flow magnitude in the absence of the pier. However, tests B8 and C10 record a slight decrease of U/U_e profiles compared to the approach flow profiles in the absence of the pier. **Figures 4.3** and **4.4** show the normalized Reynolds shear stress $-\overline{uv}/U_e^2$ profiles for both five and three sacrificial pile tests. Test E, in the absence of the pier, is provided for comparison. The majority of the tests with five and three sacrificial piles record a slight increase in the Reynolds shear stress profiles compared to test E in the absence of the pier. However, the

change in the profiles is not significant and the approach flow profiles are similar in all the experiments. Further, tests B8 and C10 profiles are almost identical to test E. **Table 4.1** shows the shear velocity for the different pier shapes, with N_p equal to number of sacrificial piles used in the respective test. The shear velocity was determined from the Reynolds shear stress profiles using the graphic method. The wall shear stress and the shear stress velocity are shown in **Equations 4.1** and **4.2**.

$$\tau_w = \rho |-uv| \quad [4.1]$$

$$U_\tau = \sqrt{\frac{\tau_w}{\rho}} \quad [4.2]$$

Table 4.1: Shear stress velocities for the different tests with various pier shapes, L/a , and N_p

Pier shape	Test ID	a (mm)	L/a	N_p	Shear velocity U_τ (mm/s)
In the absence of the pier	E	-	-	-	13.2
Sharp nose	B6	51	2	5	13.4
Round edges	B7	51	2	5	13.9
Round nose	B8	51	4	5	13.7
Round nose	C8	51	4	3	13.5
Sharp nose	C9	51	4	3	13.1
Round edges	C10	51	4	3	13.7

There is a slight increase in the shear velocities for the tests with three and five sacrificial piles compared to test E, in the absence of the pier, except for test C9. However, the shear velocities are similar in all the tests upstream of the sacrificial piles, and for test E, in the absence of the pier, and the amendment in the approach flow condition is not significant.

4.2. Scour Analysis

4.2.1. Series A: Investigation of Pier Shape and L/a Ratio on Scour Depth

This section has two distinct parts; the first subsection deals with the pier shape effect on scour depth, while the subsequent subsection will investigate the impact of the L/a ratio on scour. **Table 4.2** shows Series A results detailing the equilibrium scour depth (d_{se}), and the relative scour depth (d_{se}/a). The flow shallowness (h/a), blockage ratio (a/b), relative coarseness (a/d_{50}), Reynolds number, and Froude number were constant for all the experiments. In addition, the streamwise velocity and flow depth were recorded as $U = 0.28$ m/s and $h = 0.12$ m. Only the pier shape and

aspect ratio were varied in Series A. The geometric pier center acts as the centerline and the contour profiles' origin. Furthermore, the x -axis is in the flow direction, the y -axis is in the vertical direction, and the z -axis is transverse to the flow.

Table 4.2: Series A experimental results

Pier shape	Test ID	a (mm)	L (mm)	L/a	d_{se} (mm)	d_{se}/a
Circular	A1	51	51	1	67.4	1.32
Diamond	A2	51	51	1	53.5	1.05
Round edges	A3	51	51	1	77.6	1.52
Square	A4	51	51	1	88.9	1.75
Round nose	A5	51	102	2	56	1.1
Sharp nose	A6	51	102	2	48.5	0.95
Round edges	A7	51	102	2	59.3	1.16
Round nose	A8	51	204	4	53	1.04
Sharp nose	A9	51	204	4	39.7	0.78
Round edges	A10	51	204	4	56.8	1.11

4.2.1.1. Investigation of Pier Shape on Scour Depth

Figures 4.5 and **4.8** show the non-dimensional centreline and contour scour profiles for tests A1, A2, A3, and A4 with $L/a = 1$. The profiles for the piers with $L/a = 2$ are shown in **Figures 4.6** and **4.9**. **Figures 4.7** and **4.10** display the centerline and contour profiles for the piers with $L/a = 4$.

Figures 4.5, 4.6, and **4.7** demonstrate that the pier shape significantly affects the scour depth. It is shown in **Table 4.2** that the sharp-nosed piers with $L/a = 1, 2,$ and 4 record the minimum scour depth compared to the round-nosed and round-edged piers with the same L/a ratio. For instance, test A2 results in the minimum equilibrium scour depth for piers with $L/a = 1$. The scour depth for the diamond pier decreases by approximately 21% compared to the circular pier. In addition, there is an increase in scour depth of 66% for the square pier compared to the circular pier with $L/a = 1$. However, the round-edged pier records the maximum scour depth for piers with $L/a = 2$ and 4 . The centerline profiles indicate that the pier shape directly influences the strength of the horseshoe vortex and the separation point. Dargahi (1989) studied the connection between the separation boundaries in the sides of the pier and the vortex shedding downstream of the pier. It is found that the separation point and the separation velocity magnitude change by varying one of the parameters

affecting scour, such as blockage ratio, pier shape, and diameter. The horseshoe vortex and the separation velocity are the leading contributors and the main causes of scour development. In addition, the separation velocity affects the wake vortices strength in the downstream region.

The sharp-nosed piers have an instant bifurcation when the flow interacts with the pier nose for the different L/a ratios. As such, the minimum scour depths for $L/a = 1, 2,$ and 4 are recorded by the sharp-nosed piers. The results outcome is in tandem with Vijayasree et al. (2017), where it was shown that the sharp-nosed piers (triangular and lenticular piers) recorded the lowest scour depth, while the rectangular pier resulted in the maximum scour depth.

Figures 4.8, 4.9, and 4.10 show the contour profiles for the different pier shapes with $L/a = 1, 2,$ and $4,$ respectively. The square pier has the most significant scour hole and contour width, followed by the round-edged pier for the piers with $L/a = 1.$ Moreover, the sharp-nosed piers with $L/a = 2$ and 4 record narrower contour profiles compared to the round-nosed and round-edged piers. This is due to the pier shape, which affects the strength of the horseshoe vortex upstream of the pier and the separation velocity magnitude. Consequently, the wake vortices' strength changes with the pier shape and influences the scour hole along with the contour width in the wake region.

4.2.1.2. Investigation of L/a Ratio on Scour Depth

Figures 4.11 and 4.14 show the centerline and contour profiles for the round-nosed piers. The profiles for the sharp-nosed piers are outlined in **Figures 4.12 and 4.15,** while the centerline and contour profiles for the round-edged piers are shown in **Figures 4.13 and 4.16.**

The centerline profiles shown in **Figures 4.11, 4.12, and 4.13** demonstrate that the L/a ratio remarkably affects the scour depth. The equilibrium scour depth for piers with $L/a = 4$ is lower than the piers with $L/a = 1$ and $2.$ For instance, the scour depth decreases by 26% between the sharp-nosed pier with $L/a = 1$ and test A9 with the sharp nose and $L/a = 4.$ Additionally, the round-edged pier with $L/a = 4$ results in a scour reduction of almost 27% compared to the exact pier shape with $L/a = 1.$ The equilibrium scour depth decreases when the L/a ratio increases for similar pier shapes. As a result, there are significant changes with the pier aspect ratio for the piers with $L/a = 1$ and 2 in the downstream region. Such changes appear to be smaller for the piers with $L/a = 4.$ Piers with $L/a = 4$ have almost no scour in the wake region past the pier at $Y/a = 0.$ For example, the scour in the downstream region for the round-nosed piers significantly changes with $L/a.$ The

scour depth at $Y/a = 0$ is 50% deeper for test A1 with $L/a = 1$ than for test A5 with the round nose and $L/a = 2$, and almost 98% deeper than test A8 with $L/a = 4$. Similar observations are made for the sharp-nosed and the round-edged piers. The scour downstream of the pier decreases when the L/a ratio increases. The changes are due to the pier aspect ratio, which significantly affects the strength of the horseshoe vortex in the upstream region and the separation velocity. Further, it can be inferred that the separation velocity is affected by the pier aspect ratio, and the position of the separation changes with the pier length. The flow separation occurs due to the combination of the downward flow and the incoming flow in the sides of the pier. This separation affects the wake vortices' strength. Therefore, an increase in the L/a ratio weakens the wake vortex shedding and strength downstream of the pier.

Figures 4.14, 4.15, and 4.16 show the contour profiles for the round-nosed, sharp-nosed, and round-edged piers with different L/a ratios. The profiles have similar contour shapes for a given pier nose, particularly the downstream region of the pier. The sharp-nosed pier with $L/a = 4$ has the minimum contour width compared to tests A2 and A6 with $L/a = 1$ and 2, respectively. Similar to the sharp-nosed pier, the contour width of the round-edged pier with $L/a = 4$ slightly decreases in comparison with the same pier shape with $L/a = 1$ and 2. The similarities in the contour profiles are due to the pier shape and aspect ratio, which play a considerable role in the scour geometry. As a result, the contour width narrows down when L/a increases.

4.2.2. Investigation of Scour Reduction using Sacrificial Piles

4.2.2.1. Series B: Study of Scour Reduction using Five Sacrificial Piles

In series B, five sacrificial piles were placed at a distance $X_p = 2a$ upstream of the main pier. The main piers consisted of the different pier shapes used in Series A with $L/a = 2$ and 4. Furthermore, the diameter of the sacrificial piles was equal to 10 mm. Similar to Series A, only the pier shape and aspect ratio varied, while all other parameters were held constant. In addition, the streamwise velocity, the pier width, and the water depth were recorded as $U = 0.28$ m/s, $a = 51$ mm, and $h = 0.12$ m. **Table 4.3** shows the results from Series B, including the equilibrium scour depth, the relative scour depth, and the scour reduction. **Equation 2.3** was used to calculate the scour reduction. The equation used Series A results as the equilibrium scour depth for the unprotected pier. Series B results, using five sacrificial piles, were employed as the equilibrium

scour depth for the protected pier. The x -axis is in the flow direction, the y -axis is in the vertical direction, and the z -axis is transverse to the flow.

Table 4.3: Series B experimental results

Pier shape	Test ID	L (mm)	L/a	d_{se} (mm)	d_{se}/a	% reduction
Round nose	B5	102	2	29.2	0.57	48
Sharp nose	B6	102	2	28.7	0.56	41
Round edges	B7	102	2	31.4	0.62	47
Round nose	B8	204	4	21.6	0.42	59
Sharp nose	B9	204	4	20.8	0.41	48
Round edges	B10	204	4	22.8	0.45	60

Figures 4.17 and 4.18 show the centerline profiles for Series A tests in the absence of the sacrificial piles compared to Series B with five sacrificial piles. Table 4.3 shows that the scour depth in Series B experiments decreases by at least 40%. Further, piers with $L/a = 4$ result in greater scour reduction than piers with $L/a = 2$. For instance, the round-nosed pier (test B5) with $L/a = 2$, in the presence of the sacrificial piles, has a reduction in scour depth of 48% compared to test A5 in the absence of the scour countermeasure. On the other hand, the scour depth for the round-nosed pier (test B8) with $L/a = 4$ decreases by 59% compared to test A8. Previous research by Tafarojnoruz et al. (2012) demonstrated that the sediment scoured around the sacrificial piles is deposited and accumulated around the main pier. As a result, the presence of the sacrificial piles reduces the scour depth upstream of the main pier. In addition, the rest of the scoured sediment around the sacrificial piles and the eroded sediment around the main pier are moved to the downstream region. The wake vortices' strength also decreases in the presence of the sacrificial piles downstream of the main pier. As a result, all the experiments conducted with five sacrificial piles have positive Z/a values in the wake region of the main pier. The positive Z/a values are due to the scour countermeasure, which provides a shelter upstream of the main pier. The sacrificial piles also deflect the approach flow and reduce the horseshoe vortex effects. In addition, there is an increase in the scour reduction when the L/a ratio increases. Melville and Hadfield (1999) applied the same sacrificial pile arrangement as Series B configuration in the present investigation. Five sacrificial piles were placed in a triangular arrangement at a distance $X_p = 2a$ with $\alpha = 30^\circ$, and $S_p = 0.67a$. A scour reduction of 56% was recorded around a circular

pier. Melville and Hadfield's (1999) results and findings are similar to the results of present investigation for different pier shapes and aspect ratios.

Figures 4.19 and **4.20** show the contour profiles for Series A tests compared to Series B experiments. The two series of tests have similar contour shapes for all the piers. However, the size of the scour hole and contour profiles are narrower and shallower in Series B compared to Series A. The effects of the sacrificial piles on the scour contour can be seen in the figures. The decrease in the width of the contour shape and scour hole around the main pier is also evident for all the piers in Series B in comparison with Series A.

ADV measurements for tests in Series B (B6, B7, and B8) were acquired to further understand the approach flow characteristics upstream of the sacrificial piles. The ADV was placed at a distance equal to 0.2 m upstream of the sacrificial piles. The approach flow conditions in the absence of the pier are also provided for comparison (tests E and L). The distribution of U/U_e is shown in **Figure 4.1**. The streamwise velocity for Series B tests is similar to tests E and L, in the absence of the pier, with a slight decrease recorded by test B8. **Figure 4.3** shows the normalized Reynolds shear stress profiles. The $-\overline{uv}/U_e^2$ profiles for Series B tests are almost the same as test E in the absence of the pier. **Table 4.1** shows the shear velocities obtained from the Reynolds shear stress profiles using the graphic method. There is a slight change in the Reynolds shear stress profiles and the shear velocities between Series B experiments and test E. However, the changes are not significant and the approach flow profiles are almost the same in all the tests. The slight change in the profiles could be due to measurement errors, variation in the measurement locations between Series B tests and test E, in the absence of the pier, and the flow adjustment to the presence of the piles.

4.2.2.2 Series C: Study of Scour Reduction using Three Sacrificial Piles

Three sacrificial piles were placed at a distance $X_p = 2a$ upstream of the main pier in Series C. The main piers consisted of the different pier shapes used in Series A with $L/a = 2$ and 4. The diameter of the sacrificial piles was equal to 10 mm and the spacing between the sacrificial piles $S_p = a$. The dimensionless parameters remained constant except for the pier shape and aspect ratio in Series C. Moreover, the streamwise velocity, the pier width, and the water depth were equal to $U = 0.28$ m/s, $a = 51$ mm, and $h = 0.12$ m, respectively. **Table 4.4** shows the experimental results from Series C, including the equilibrium scour depth, the relative scour depth, and the scour

reduction. **Equation 2.3** was used to calculate the scour reduction. The results from Series A were used as the equilibrium scour depth for the unprotected pier in the equation. Series C results using three sacrificial piles were employed as the equilibrium scour depth for the protected pier. The x -axis is in the flow direction, the y -axis is in the vertical direction, and the z -axis is transverse to the flow.

Table 4.4: Series C experimental results

Pier shape	Test ID	L (mm)	L/a	d_{se} (mm)	d_{se}/a	% reduction
Round nose	C5	102	2	27.9	0.55	50
Sharp nose	C6	102	2	21.7	0.43	55
Round edges	C7	102	2	25.7	0.5	57
Round nose	C8	204	4	19.9	0.39	62
Sharp nose	C9	204	4	18.6	0.37	53
Round edges	C10	204	4	20.5	0.4	64

Figures 4.21 and **4.22** show the centerline profiles for Series A tests in the absence of the sacrificial piles compared to Series C tests with three sacrificial piles. **Table 4.4** shows that the scour depth decreases by at least 50% in Series C tests compared to Series A. In addition, piers with $L/a = 4$ have a higher scour reduction than piers with $L/a = 2$. The results demonstrate the effect of the L/a ratio on scour reduction, where the scour reduction increases when there is an increase in the pier aspect ratio. Further, the minimum scour depth in the present investigation is recorded by test C9 among all the experiments in Series A, B, and C. The findings show that the use of three sacrificial piles is efficient in deflecting the approach flow and reducing the horseshoe vortex. Thereby, this arrangement results in a better protection of the main pier. Chang and Karim (1972) used the same pile arrangement with $N_p = 3$, $X_p = 2a$, and $S_p = a$. A maximum scour decrease of 65% was recorded. The scour reduction for the different piers in the present investigation is similar to Chang and Karim (1972) results and findings, where the scour depths of the round-nosed and round-edged piers with $L/a = 4$ decrease by more than 60%.

Figures 4.23 and **4.24** show the contour profiles for Series A tests compared to Series C experiments. The contour profiles have a similar contour shape between Series A and Series C tests. However, Series C results record a reduced contour width compared to Series A tests. It can be demonstrated from the contour profiles that the three sacrificial piles reduce the horseshoe

vortex effect upstream of the pier as they weaken the wake vortices strength downstream of the main pier.

To further understand the approach flow characteristics, ADV measurements were taken upstream of the sacrificial piles. The ADV was placed at a distance equal to 0.2 m upstream of the sacrificial piles for tests C8, C9, and C10 with $L/a = 4$. The approach flow profiles in the absence of the pier are also provided for comparison (tests E and L). The distribution of the streamwise velocity shown in **Figure 4.2** demonstrates that Series C tests are similar to tests E and L in the absence of the pier with a slight decrease for test C10. **Figure 4.4** shows the normalized Reynolds shear stress profiles against z/h . Series C tests have similar $-\overline{uv}/U_e^2$ profiles as test E in the absence of the pier. Further, **Table 4.1** shows that the shear velocity is almost identical for all the tests in Series C as well as test E. The changes in the approach flow profiles are minor upstream of the sacrificial piles and the approach flow is almost the same for all the tests. Similar to Series B tests, the negligible amendments are mainly due to device errors, and the change in the measurement location between tests with sacrificial piles and experiments in the absence of the pier.

4.2.2.3 Comparison between Series B and Series C Experiments

In Series B, five sacrificial piles were used, while Series C tests had three piles. The distance X_p was equal to $2a$, while the sacrificial pile diameter was $D_p = 10$ mm. **Table 4.5** shows the results of both series of tests, including the equilibrium scour depth, the relative scour depth, and the scour reduction calculated from **Equation 2.3**. Here d_{se0} represents the maximum scour depth from Series B tests, and the results from Series C were used for d_{se} in **Equation 2.3**. The investigation assumed that the number of sacrificial piles N_p , the lateral spacing between the piles S_p , pier shape, and the L/a ratio varied while the other parameters were constant.

Table 4.5: Comparison between Series B and Series C results and scour reduction percentage in Series C compared to Series B

Pier shape	Test ID	L (mm)	L/a	d_{se} (mm)	d_{se}/a	%reduction
Round nose	B5	102	2	29.7	0.57	-
	C5	102	2	27.9	0.55	6
Sharp nose	B6	102	2	28.7	0.56	-
	C6	102	2	21.7	0.43	24
Round edges	B7	102	2	31.4	0.62	-
	C7	102	2	25.7	0.5	18
Round nose	B8	204	4	21.6	0.42	-
	C8	204	4	19.9	0.39	8
Sharp nose	B9	204	4	20.8	0.41	-
	C9	204	4	18.6	0.37	11
Round edges	B10	204	4	22.8	0.45	-
	C10	204	4	20.5	0.4	10

Figures 4.25 and 4.26 provide the centerline profiles of Series B compared to Series C with $L/a = 2$ and 4, respectively. The experimental results show that the round-nosed piers with $L/a = 2$ and 4 in both series of tests have almost the same equilibrium scour depth. However, the scour reduction for Series C is better than Series B for the sharp-nosed and round-edged piers. For instance, test C6 has a scour reduction of 24% compared to B6. It is evident that the use of three sacrificial piles produces lower scour depth than using five piles. It can be inferred that the three sacrificial piles facilitate the transport of the scoured sediment from the upstream to the downstream region of the sacrificial piles. Consequently, the sediment is moved to the upstream region of the main pier. In addition, all the piers in the two series of tests have positive Z/a values for the different piers. Therefore, using the sacrificial piles plays a considerable role in lowering the wake vortices effect by reducing the strength of the horseshoe vortex, and deflecting the approach flow upstream of the sacrificial piles.

Figures 4.27 and 4.28 show the contour profiles in Series B and Series C tests. The contour shapes are similar for all the piers and L/a ratios. However, Series C tests have a slight decrease in the contour and scour hole width compared to Series B tests. The similarities in the contour

profiles are mainly due to the pier shape. Further, the use of sacrificial piles reduces the effect of the horseshoe vortex. Consequently, the contour shape and width are similar with a slight decrease recorded by Series C tests.

4.3. Development of a New Scour Estimation Method

The flow shallowness (h/a), the flow intensity (U/U_c), and the relative coarseness (a/d_{50}) are previously used to estimate the scour depth. However, Hodi (2009) showed that the densimetric Froude number affected the scour depth around circular piers. It was also found that the scour depth and geometry changed vastly for a relatively small change in F_d . The densimetric Froude number represents the flow-sediment interactions (**Equation 4.3**), as shown below:

$$F_d = \frac{U}{\sqrt{g(SG-1)d_{50}}} \quad [4.3]$$

In **Equation 4.3**, U is the streamwise velocity, SG represents the specific gravity of the sediment, g is the acceleration due to gravity, and d_{50} is the mean sediment diameter. Further, Williams (2014) studied the effect of the blockage ratio (a/b) and the separation velocity on scour depth. The scour estimation method developed at the University of Windsor was an empirical equation (**Equation 4.4**).

$$\frac{d_{se}}{a} = 1.01(F_{ds})^{-0.284} \left(\frac{h}{a}\right)^{0.325} \left(\frac{a}{d_{50}}\right)^{0.059} \quad [4.4]$$

In **Equation 4.4**, the flow velocity in F_d is replaced with U_s , yielding a new F_{ds} term. The velocity at the point of separation is known as separation velocity U_s , and it highly influences the scour depth (Williams et al., 2016). In the present investigation, it has been noted that the location of the separation point and the separation velocity magnitude change with the pier shape and aspect ratio. As previously described in Section 2, in a fully turbulent flow, the flow velocity increases upstream of the pier and forms a stagnation point with a decreasing pressure towards the bed. Dargahi (1990) investigated the scour mechanism around the pier and the connection between the separation boundary layer upstream of the pier and the periodic vortex shedding in the wake region. The study showed that the separation occurred when the pressure gradient caused by the pier was overcome by the boundary layer in the upstream region. The point of separation changes with varying one of the parameters affecting scour, such as the blockage ratio, pier shape and diameter. The separation point is at the edges of the pier, and it is reached when the separation velocity profiles are flattened. The velocity reaches the maximum value at the

separation point, where the downward flow and the incoming flow combine around the pier and result in the formation of the horseshoe vortex and flow separation from the pier.

To further understand the effect of the pier shape on the separation velocity, four tests using the ADV were carried out. The measurements were performed along the midpoint between the center of the pier and the sidewall. The ADV was placed at $X = 3.5$ m from the boundary layer trip, $Y = -b/4$ m from the centerline, and at a depth $Z = 0.35$ m, as shown in **Figure 3.7**. The gap between a given test's measurements was equal to 0.02 m in the streamwise direction. **Figure 4.29** outlines the velocity in the separation region for tests A4 with $L/a = 1$ and tests A8, A9, and A10 with $L/a = 4$. The velocity profiles are normalized by the velocity at the location $X = 3.5$ m, $Y = -b/4$, and $Z = 0.35$ m in the absence of the pier, while the x -axis is normalized by the pier width $a = 51$ mm. **Figure 4.29** shows that the sharp-nosed pier with $L/a = 4$ reaches the separation point slightly quicker than the round-nosed and round-edged piers with $L/a = 4$; by contrast, the velocity magnitude of the square pier is still increasing in the x -direction, and the separation point is not yet reached. It can be inferred from the figure that the position of the separation velocity point changes with the pier shape.

The present investigation demonstrated that there are two additional parameters affecting the scour depth, which are the pier shape and aspect ratio. **Figure 4.30** shows that the equilibrium scour depth changes with the pier shape and L/a value. With an increase in the pier aspect ratio, d_{se}/a decreases. Further, the scour depth changes with the pier shape nose. These two factors may not be of the highest importance in scour prediction, but they still affect the equilibrium scour depth and therefore must be incorporated into scour estimation.

The influence of the flow shallowness and the relative coarseness on scour depth are evident in literature. Further, the general trend of the relationship between each parameter and d_{se}/a is exponential (Williams, 2014). Based on the previous investigations at the University of Windsor, where **Equation 4.4** was developed, the parameters chosen for the current scour estimation method are h/a , a/d_{50} , L/a , K_{sh} , and F_{ds} . The pier shape factor K_{sh} for the different piers is shown in **Table 2.1**. The densimetric Froude number is a function of the separation velocity (**Equation 4.5**) and the form of the equation is shown in **Equation 4.6**.

$$F_{ds} = \frac{U_s}{\sqrt{g(SG-1)d_{50}}} \quad [4.5]$$

$$\frac{d_{se}}{a} = C(F_{ds})^{n_1} \left(\frac{h}{a}\right)^{n_2} \left(\frac{a}{d_{50}}\right)^{n_3} \left(\frac{L}{a}\right)^{n_4} \quad [4.6]$$

Various investigations were used to develop the scour estimation method, including Ettema et al. (2006), Williams (2014), Vijayasree et al. (2017), and the results of the current investigation. Using the solver tool in Microsoft Excel, the values of the different n exponents and the constant C in **Equation 4.6** were determined. The developed estimation method is shown in **Equation 4.7**.

$$\frac{d_{se}}{a} = 1.178 (F_{ds})^{0.293} \left(\frac{h}{a}\right)^{0.186} \left(\frac{a}{d_{50}}\right)^{-0.078} \left(\frac{L}{a}\right)^{-0.016} K_{sh} \quad [4.7]$$

Figure 4.31 shows the graphical relationship between the measured and the predicted equilibrium scour depths using **Equation 4.7**, grouped by study. In **Figures 4.31** and **4.32**, $(d_{se}/a)_m$ indicates the measured value of the scour, and $(d_{se}/a)_p$ represents the predicted equilibrium scour depth using the scour estimation methods. The outline of the results shows that the trend is reasonable and similar to the line of perfect agreement. The equation does not tend to significantly over or under predict the equilibrium scour depth. **Figure 4.32** shows the graphical relationship between the measured and predicted equilibrium scour depths using the HEC-18 equation. The HEC-18 equation is the most used scour estimation method in North America for bridge pier design. This estimation method tends to over-predict the scour depth for the different investigations shown in the figure, especially for the results of Vijayasree et al. (2017).

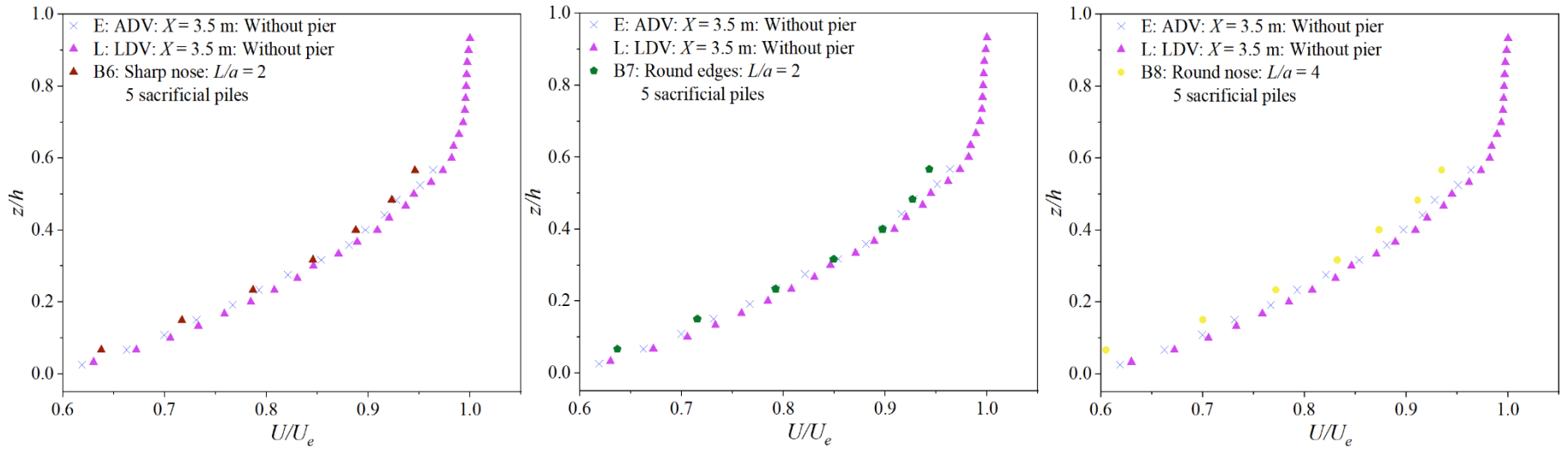


Figure 4.1: Streamwise velocity U profiles for tests B6, B7, and B8 with five sacrificial piles compared to tests E and L in the absence of the pier

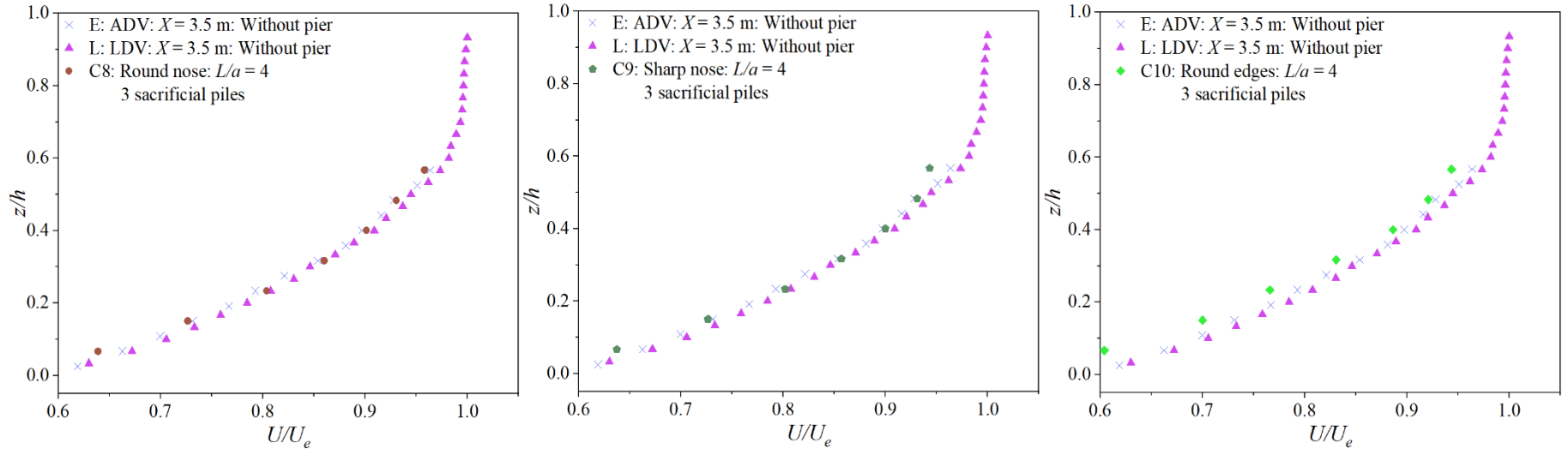


Figure 4.2: Streamwise velocity U profiles for tests C8, C9, and C10 with three sacrificial piles compared to tests E and L in the absence of the pier

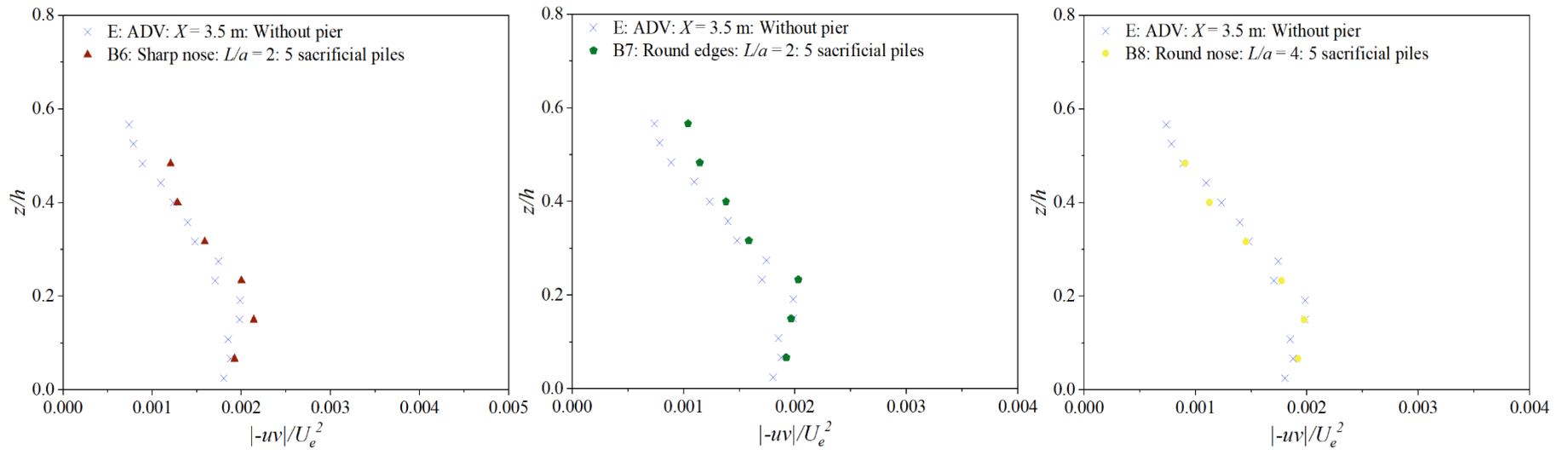


Figure 4.3: Reynolds shear stress profiles for tests B6, B7, and B8 with five sacrificial piles compared to test E in the absence of the pier

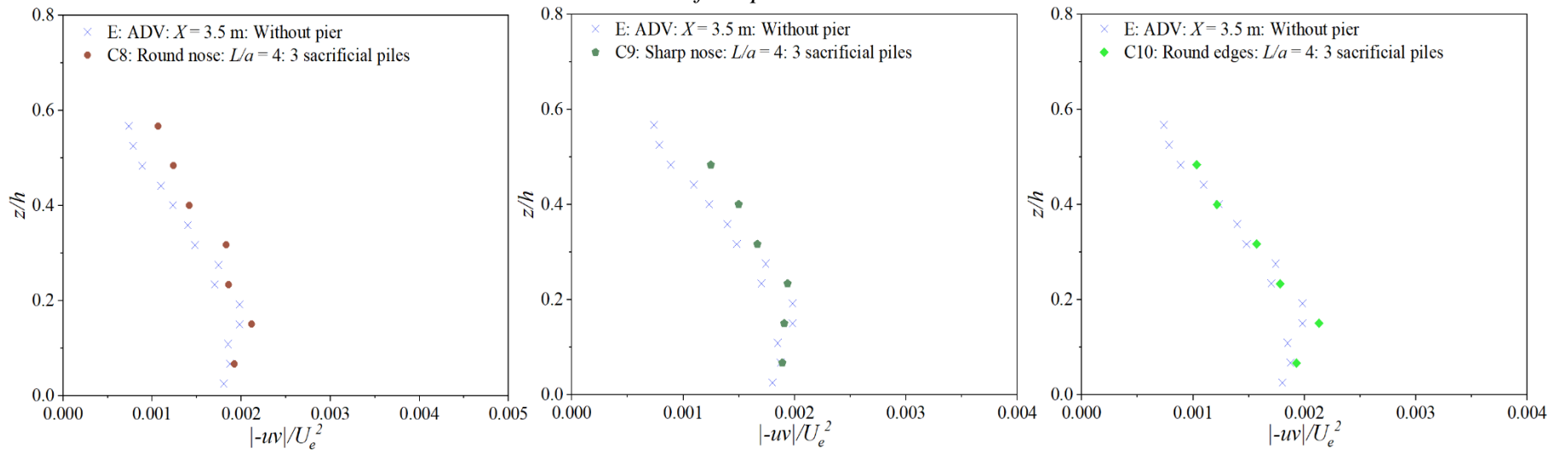


Figure 4.4: Reynolds shear stress profiles for tests C8, C9, and C10 with three sacrificial piles compared to test E in the absence of the pier

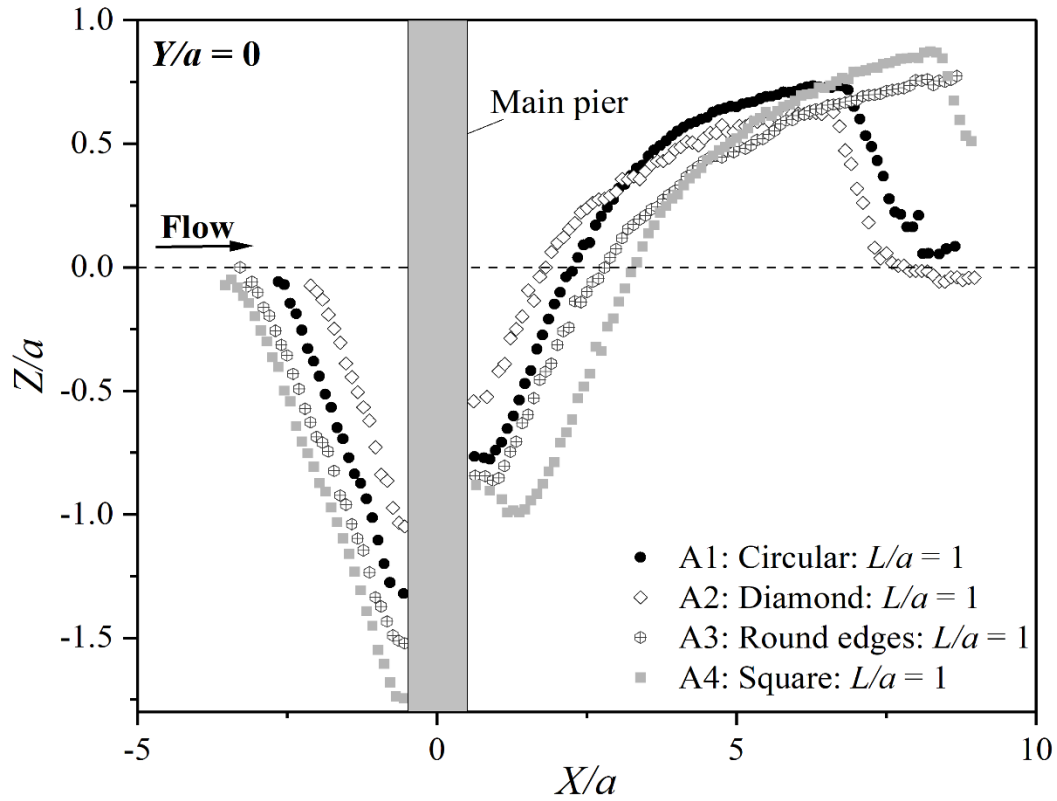


Figure 4.5: Centerline profiles of the piers with $L/a = 1$ (A1, A2, A3, and A4)

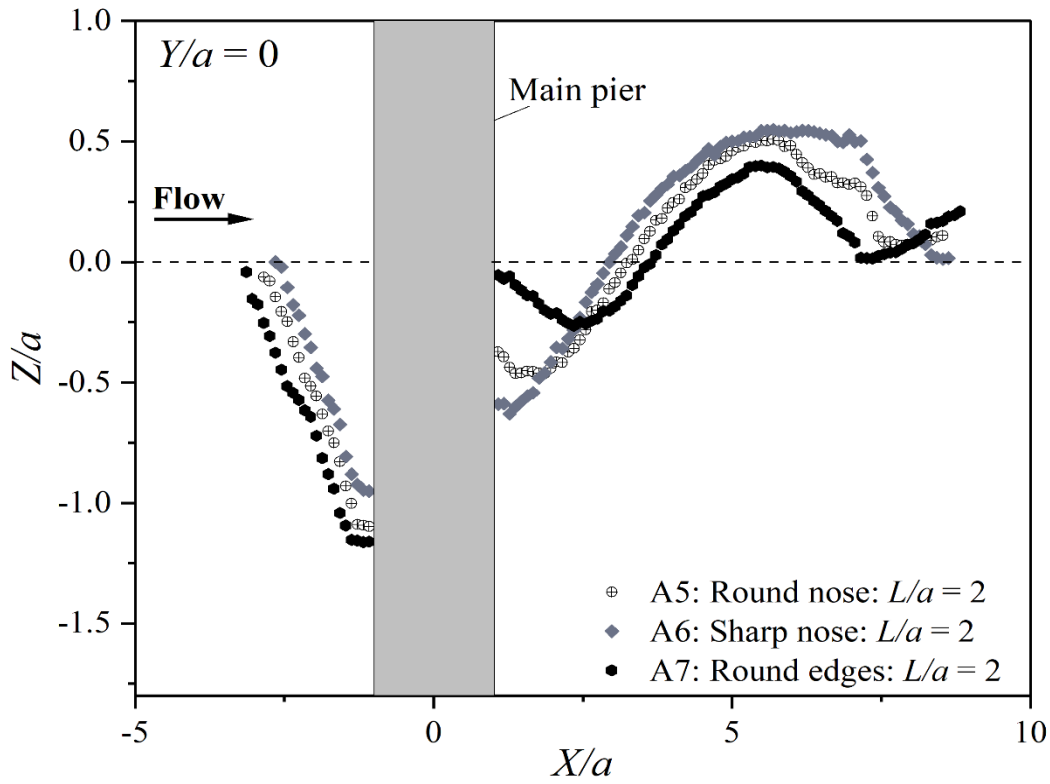


Figure 4.6: Centerline profiles of the piers with $L/a = 2$ (A5, A6, and A7)

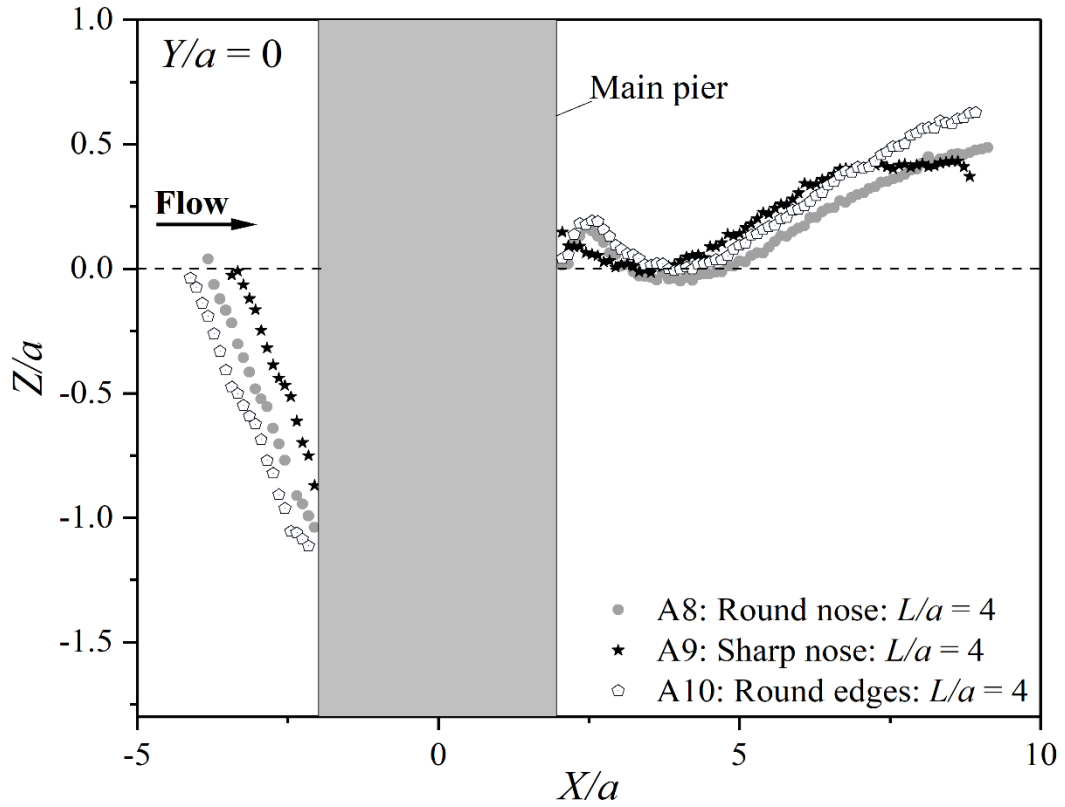


Figure 4.7: Centerline profiles of the piers with $L/a = 4$ (A8, A9, and A10)

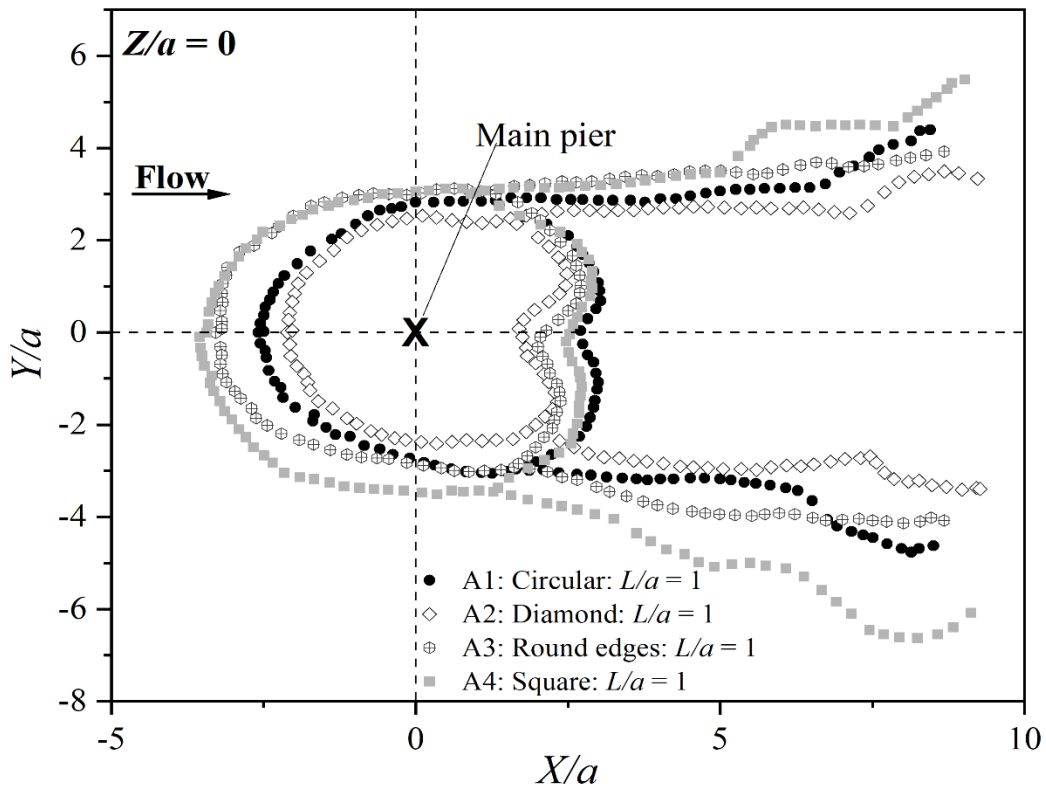


Figure 4.8: Contour profiles of the piers with $L/a = 1$ (A1, A2, A3, and A4)

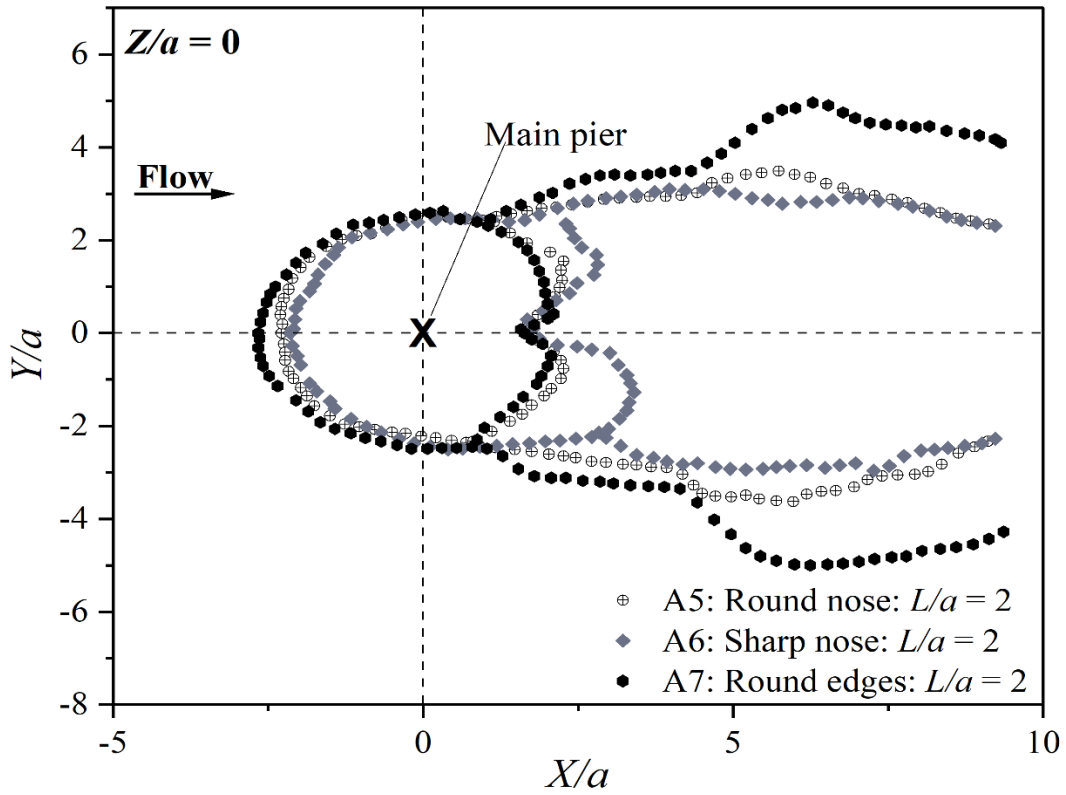


Figure 4.9: Contour profiles of the piers with $L/a = 2$ (A5, A6, and A7)

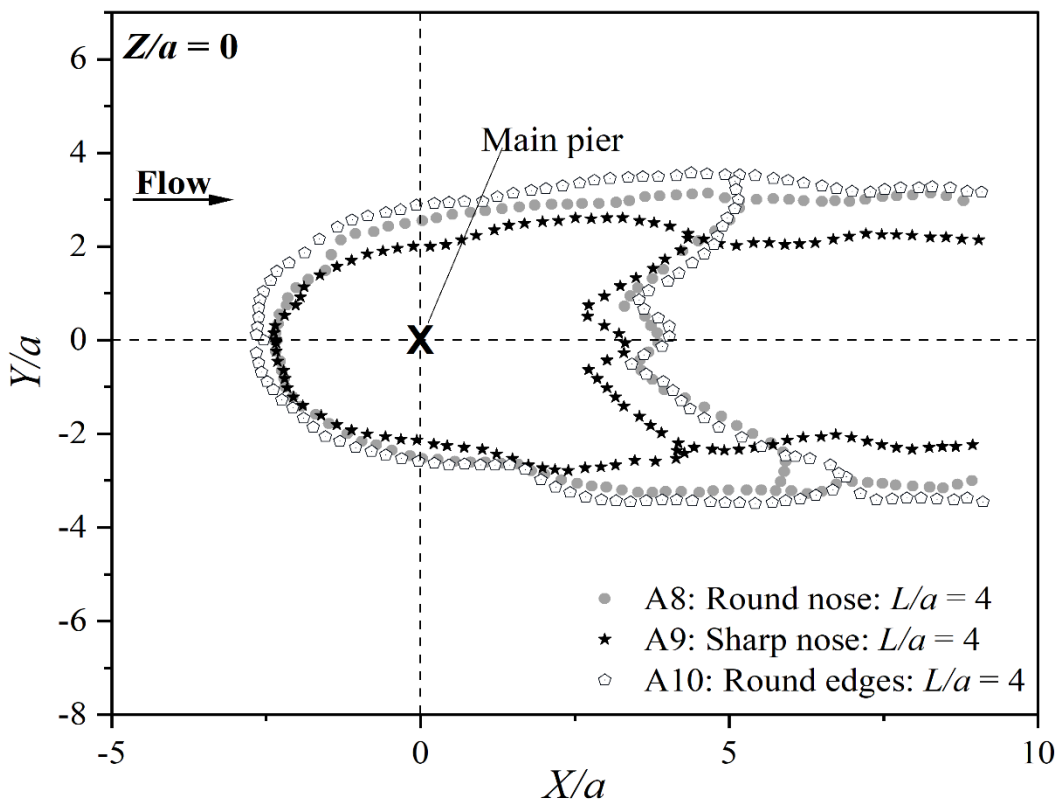


Figure 4.10: Contour profiles of the piers with $L/a = 4$ (A8, A9, and A10)

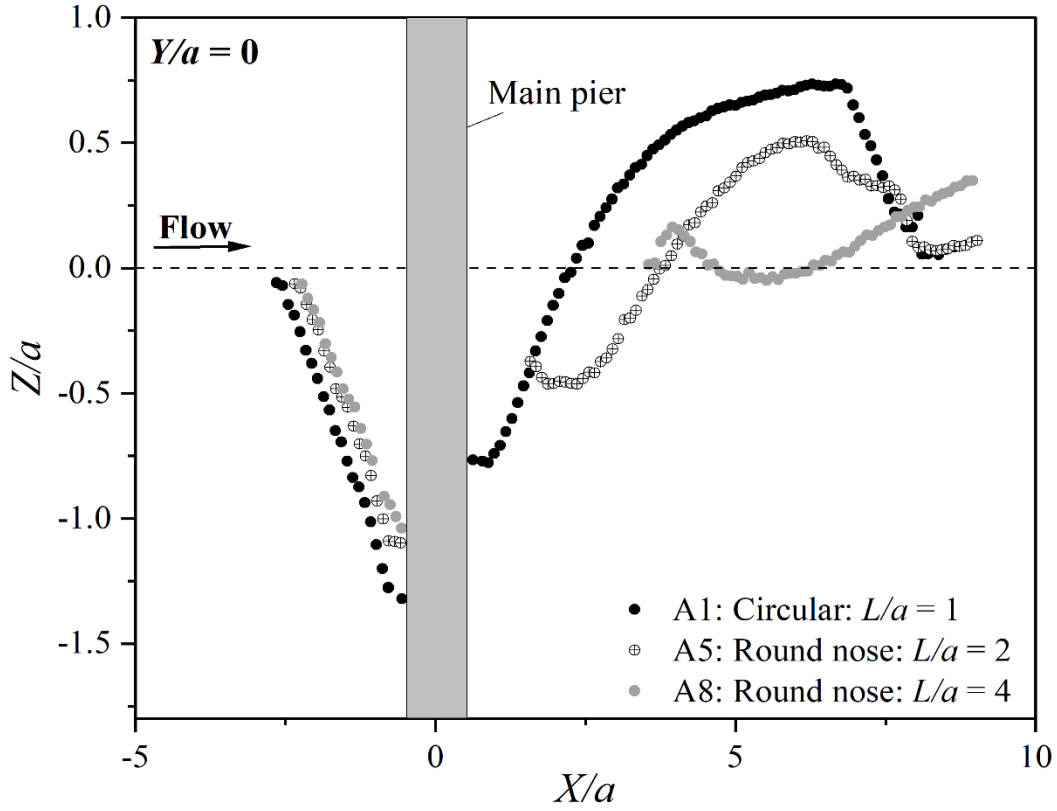


Figure 4.11: Centerline profiles of round-nosed piers (A1: $L/a = 1$, A5: $L/a = 2$, and A8: $L/a = 4$)

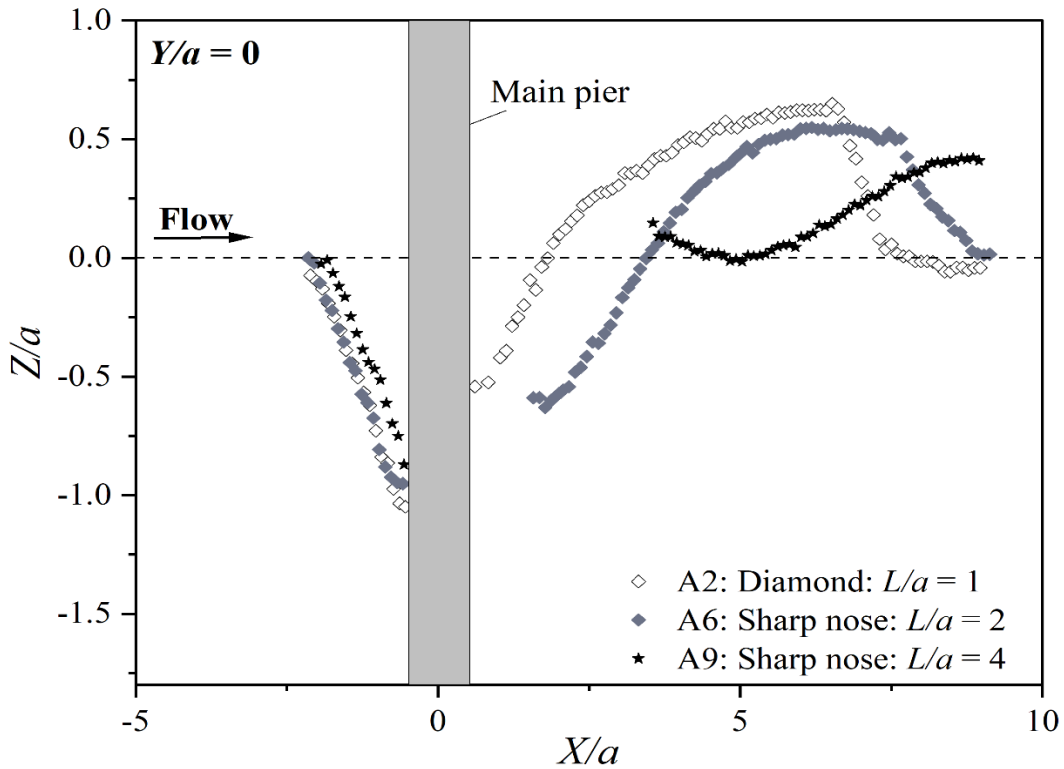


Figure 4.12: Centerline profiles of sharp-nosed piers (A2: $L/a = 1$, A6: $L/a = 2$, and A9: $L/a = 4$)

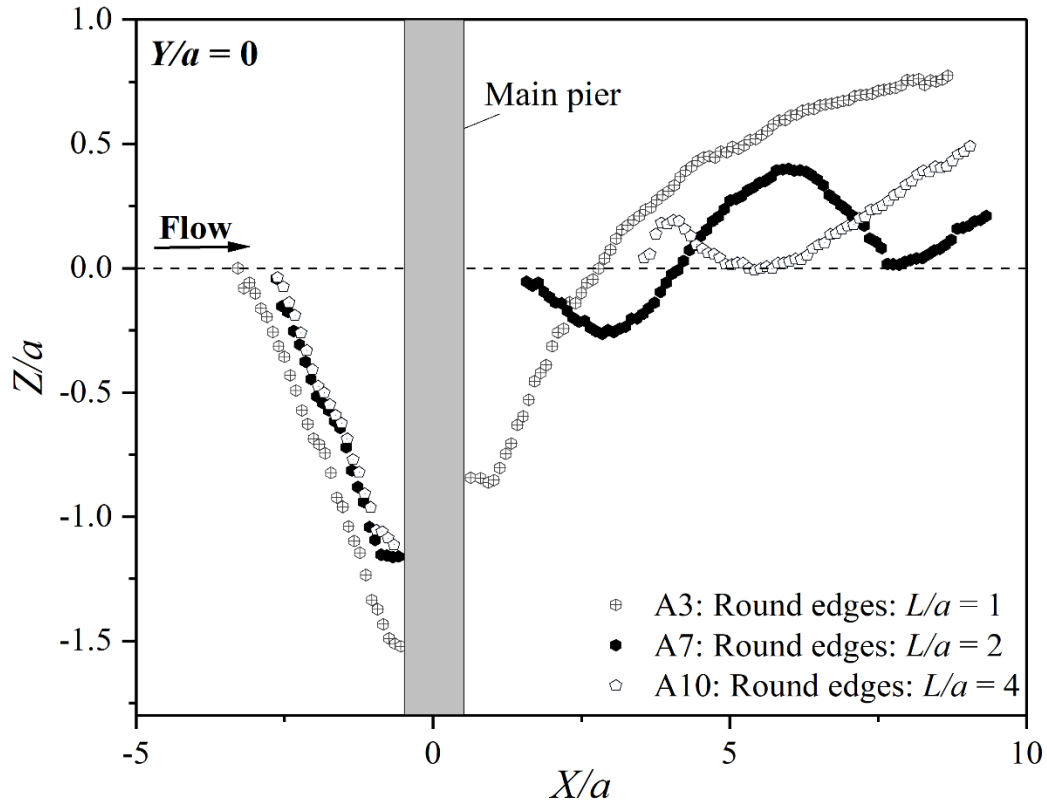


Figure 4.13: Centerline profiles of round edged piers (A3: $L/a = 1$, A7: $L/a = 2$, and A10: $L/a = 4$)

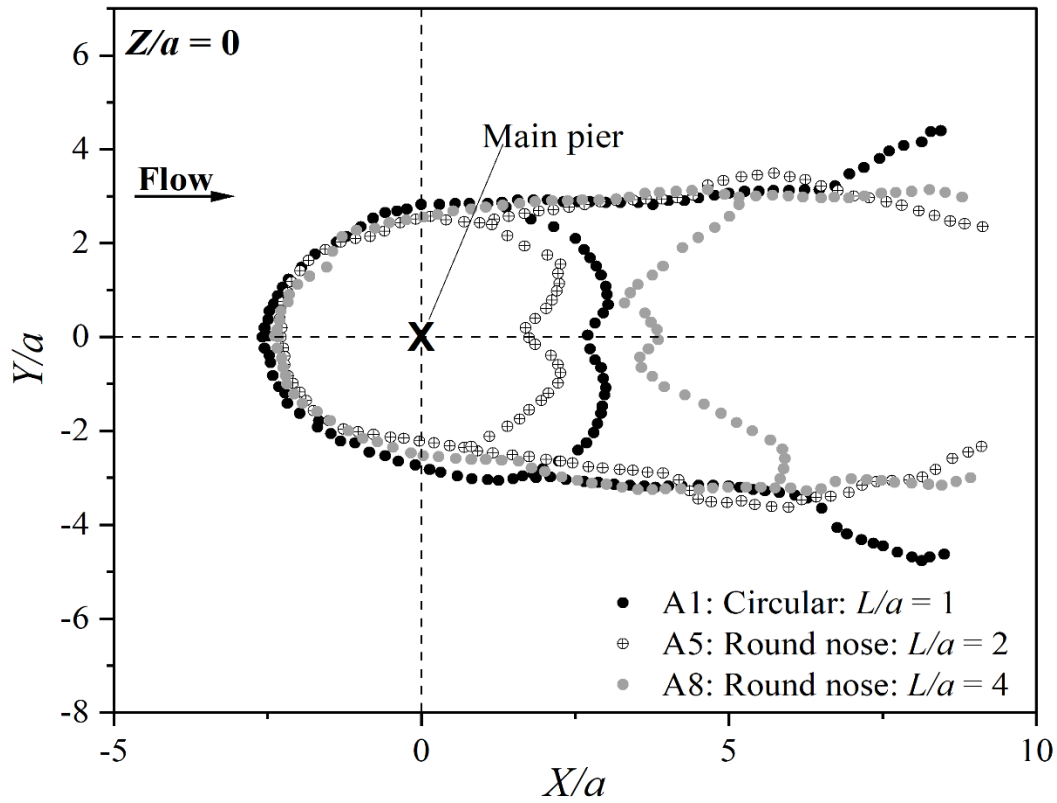


Figure 4.14: Contour profiles of round-nosed piers (A1: $L/a = 1$, A5: $L/a = 2$, and A8: $L/a = 4$)

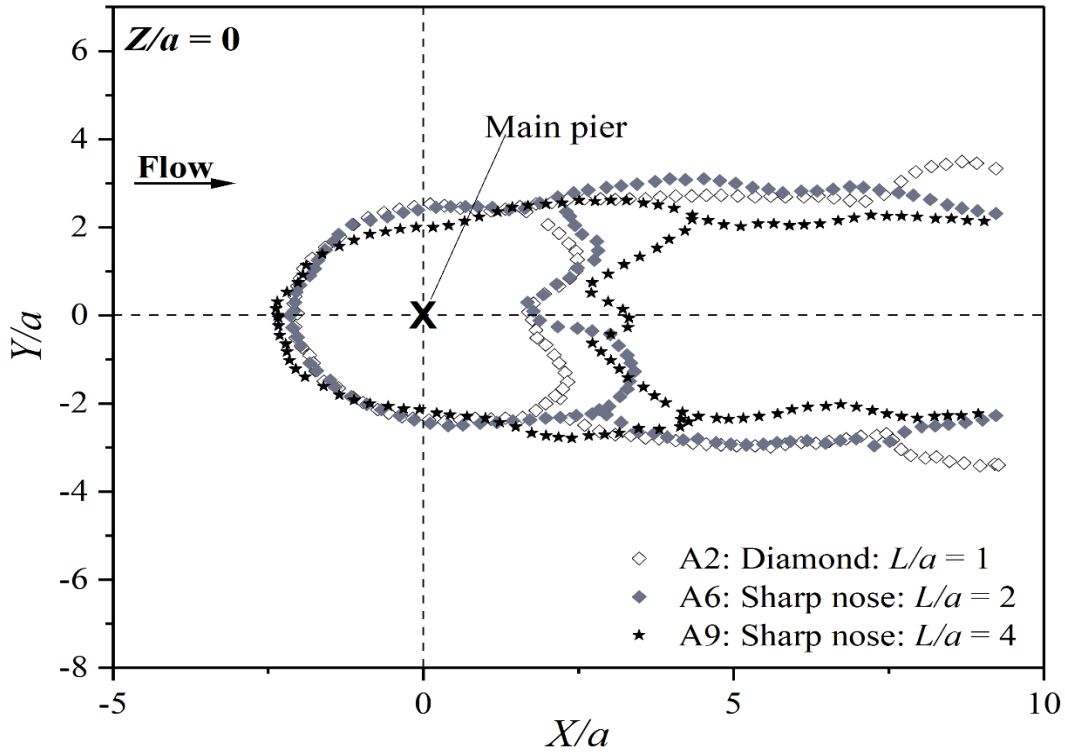


Figure 4.15: Contour profiles of sharp-nosed piers (A2: $L/a = 1$, A6: $L/a = 2$, and A9: $L/a = 4$)

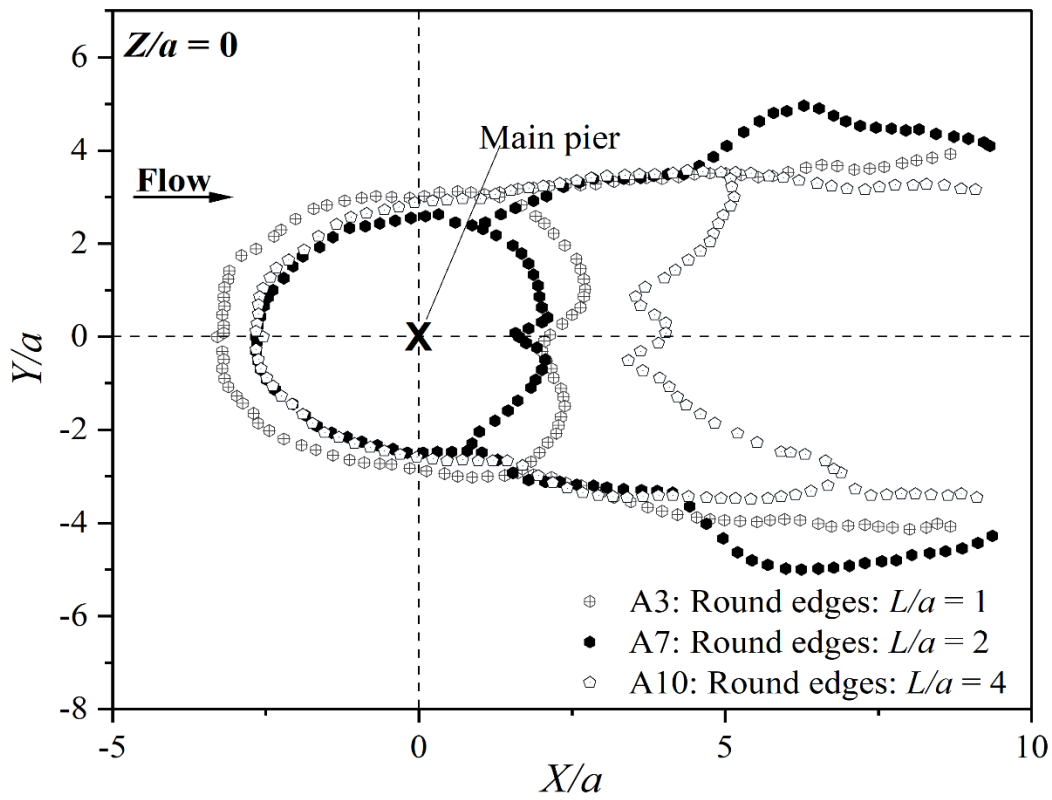


Figure 4.16: Contour profiles of round-edged piers (A3: $L/a = 1$, A7: $L/a = 2$, and A10: $L/a = 4$)

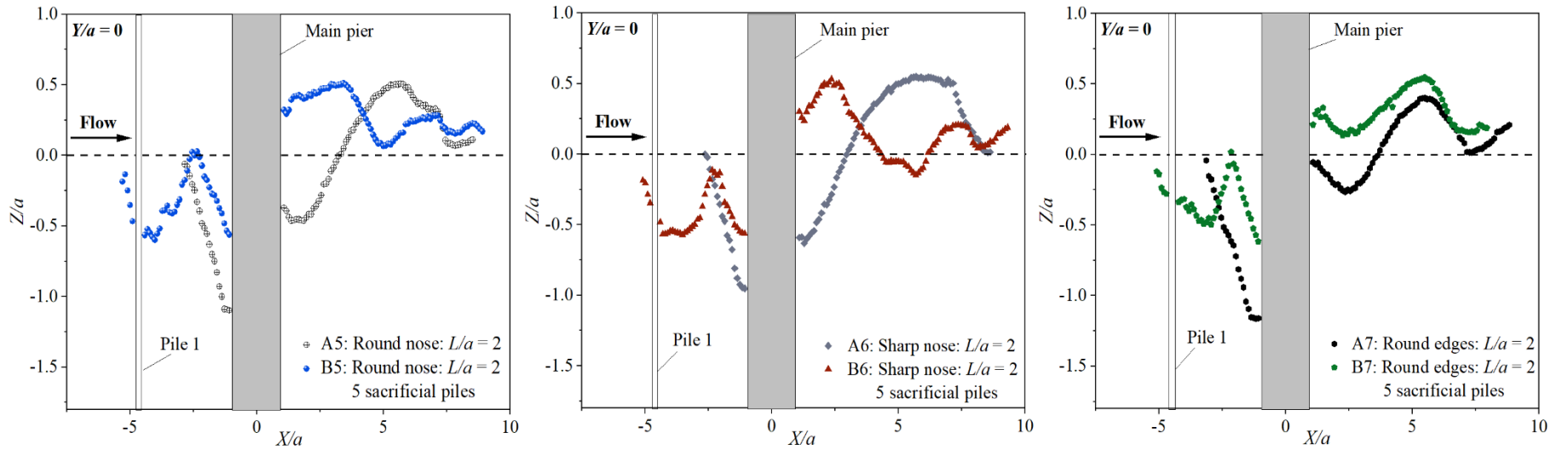


Figure 4.17: Centerline profiles for piers with $L/a = 2$ with and without five sacrificial piles (tests A5, A6, and A7 without sacrificial piles, and tests B5, B6, and B7 with five sacrificial piles)

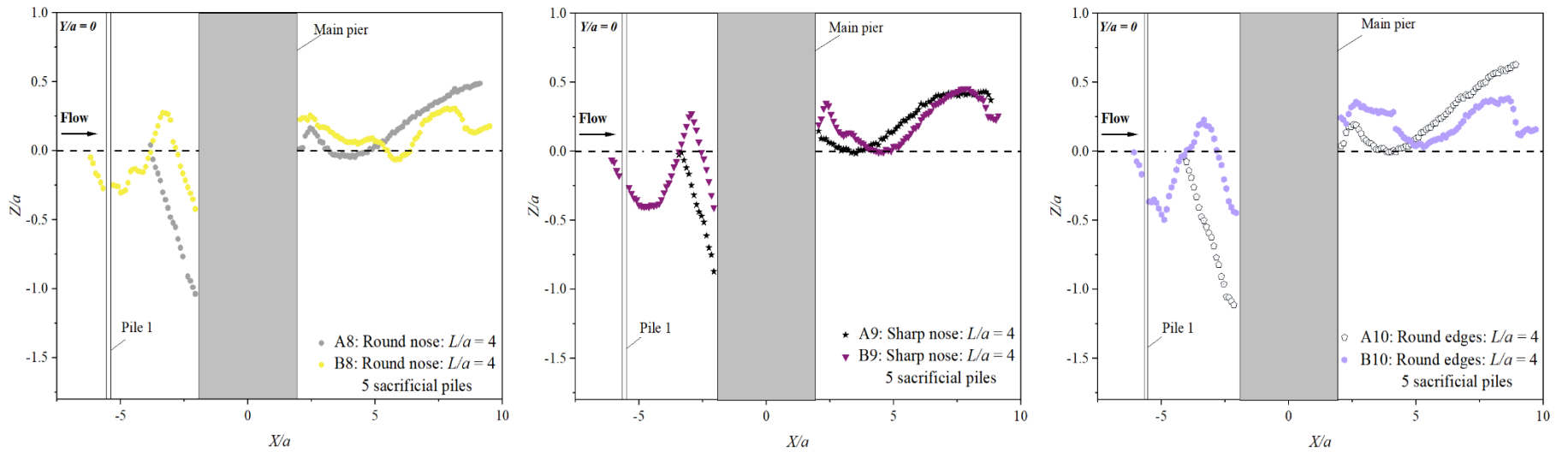


Figure 4.18: Centerline profiles for piers with $L/a = 4$ with and without five sacrificial piles (tests A8, A9, and A10 without sacrificial piles, and tests B8, B9, and B10 with five sacrificial piles)

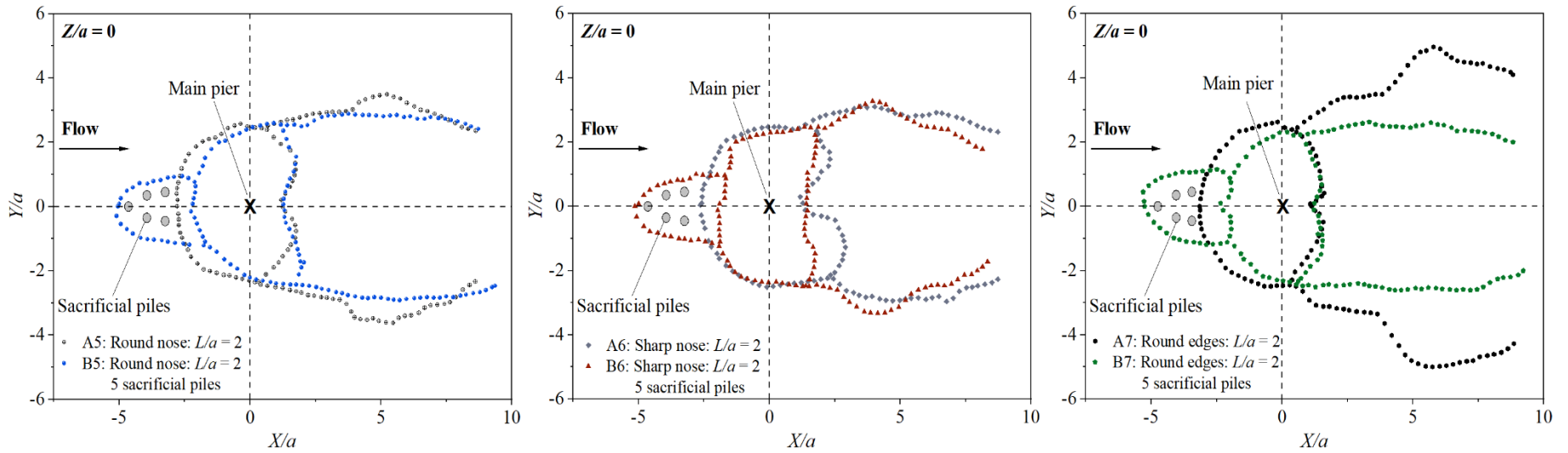


Figure 4.19: Contour profiles for piers with $L/a = 2$ with and without five sacrificial piles (tests A5, A6, and A7 without sacrificial piles, and tests B5, B6, and B7 with five sacrificial piles)

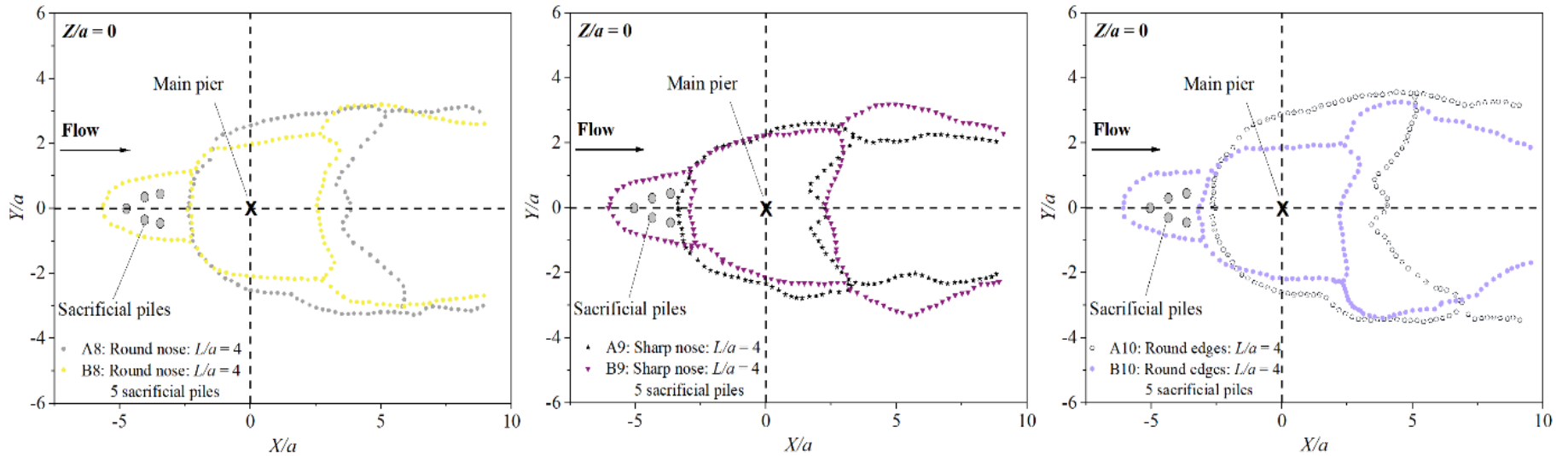


Figure 4.20: Contour profiles for piers with $L/a = 4$ with and without five sacrificial piles (tests A8, A9, and A10 without sacrificial piles, and tests B8, B9, and B10 with five sacrificial piles)

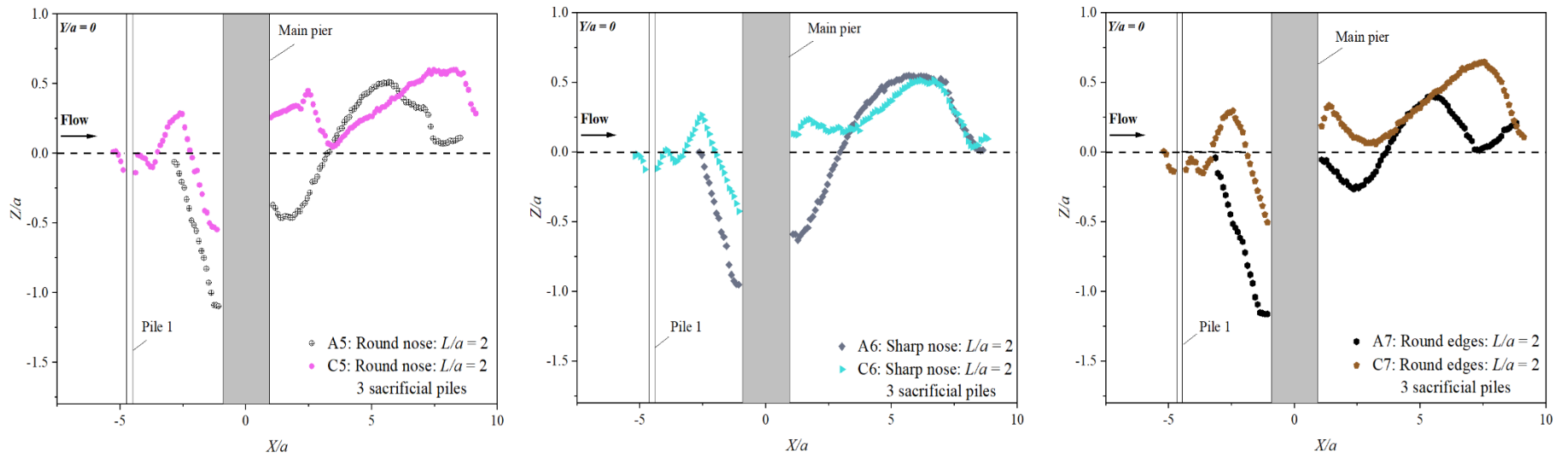


Figure 4.21: Centerline profiles for piers with $L/a = 2$ with and without three sacrificial piles (tests A5, A6, and A7 without sacrificial piles, and tests C5, C6, and C7 with three sacrificial piles)

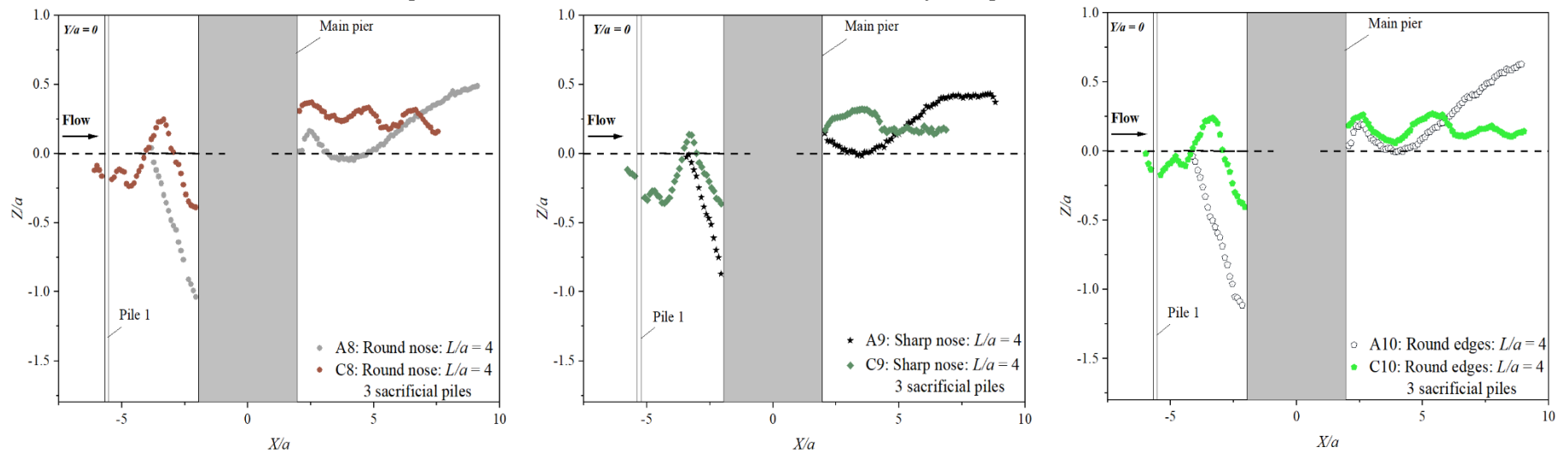


Figure 4.22: Centerline profiles for piers with $L/a = 4$ with and without three sacrificial piles (tests A8, A9, and A10 without sacrificial piles, and tests C8, C9, and C10 with three sacrificial piles)

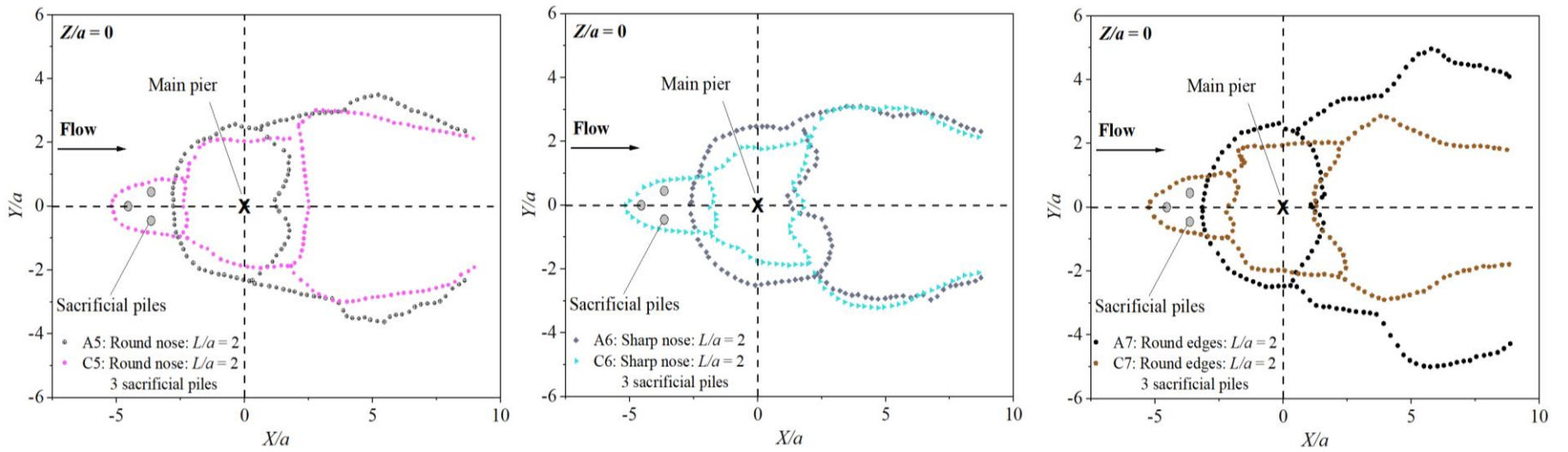


Figure 4.23: Contour profiles for piers with $L/a = 2$ with and without three sacrificial piles (tests A5, A6, and A7 without sacrificial piles, and tests C5, C6, and C7 with three sacrificial piles)

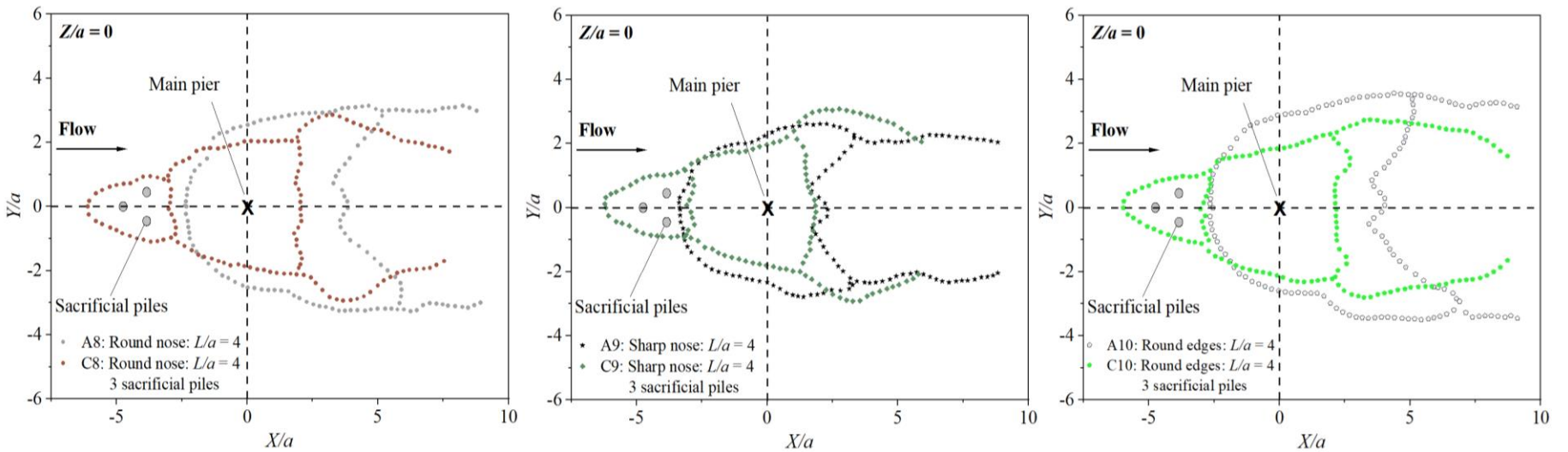


Figure 4.24: Contour profiles for piers with $L/a = 4$ with and without three sacrificial piles (tests A8, A9, and A10 without sacrificial piles, and tests C8, C9, and C10 with three sacrificial piles)

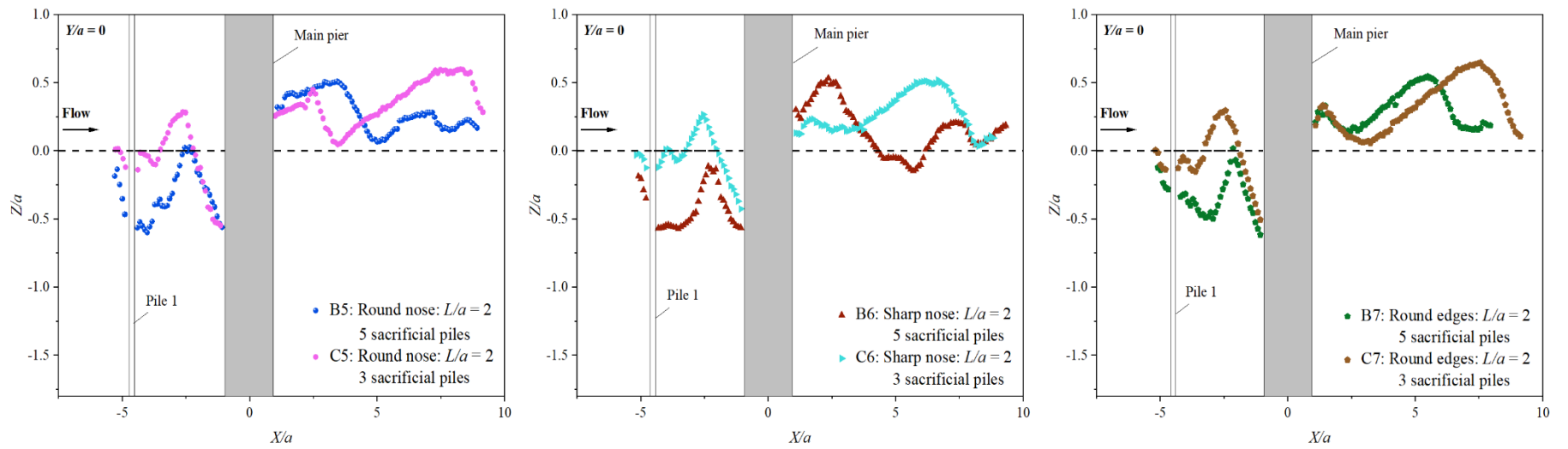


Figure 4.25: Centerline profiles for $L/a = 2$ in Series B and Series C with five and three sacrificial piles (tests: B5, B6, and B7 with five sacrificial piles, and tests C5, C6, and C7 with three sacrificial piles)

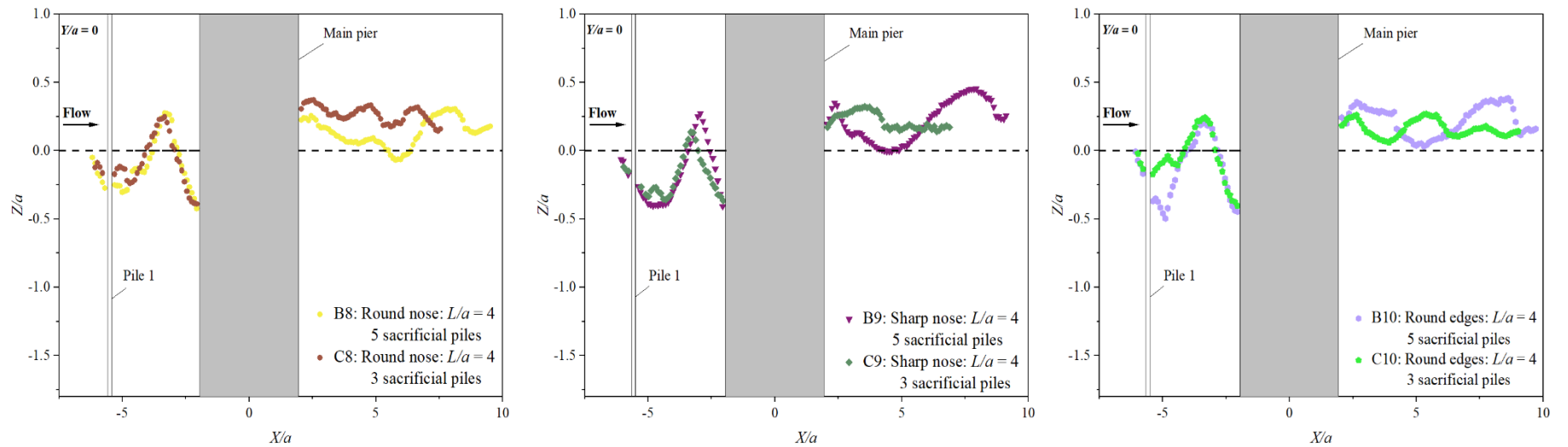


Figure 4.26: Centerline profiles for $L/a = 4$ in Series B and Series C with five and three sacrificial piles (tests: B8, B9, and B10 with five sacrificial piles, and tests C8, C9, and C10 with three sacrificial piles)

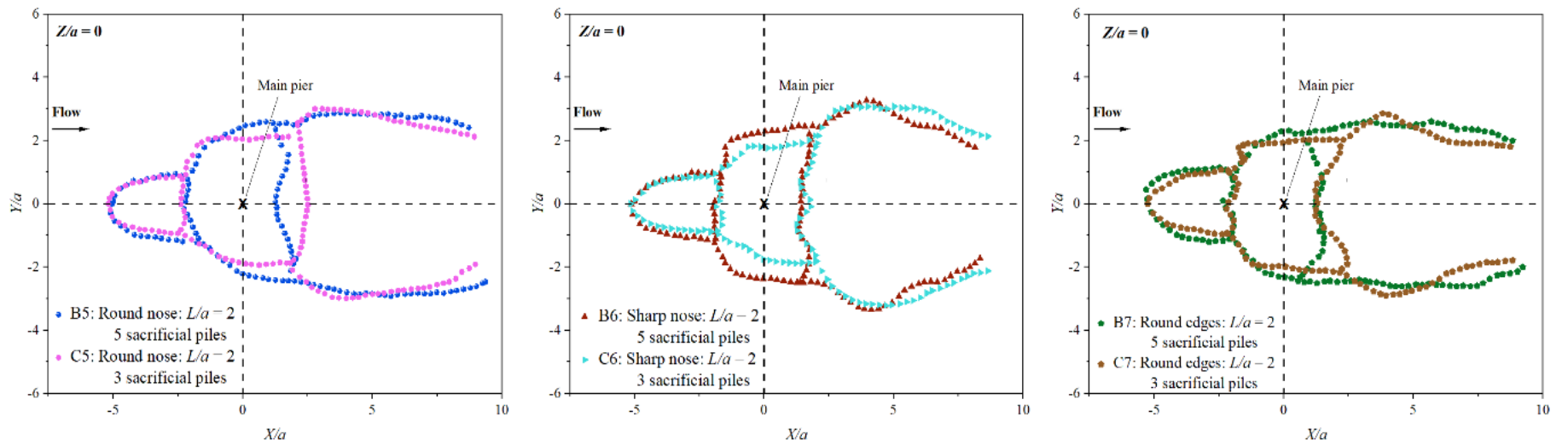


Figure 4.27: Contour profiles for piers with $L/a = 2$ in Series B and Series C with five and three sacrificial piles (tests B5, B6, and B7 with five sacrificial piles, and tests C5, C6, and C7 with three sacrificial piles)

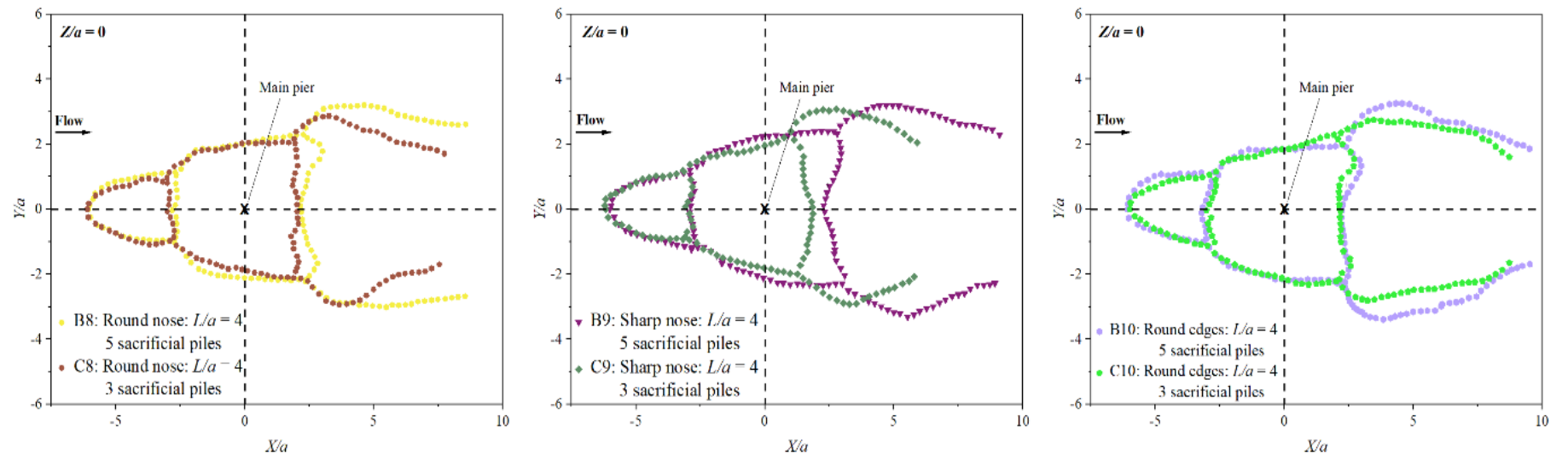


Figure 4.28: Contour profiles for piers with $L/a = 4$ in Series B and Series C with five and three sacrificial piles (tests B8, B9, and B10 with five sacrificial piles, and tests C8, C9, and C10 with three sacrificial piles)

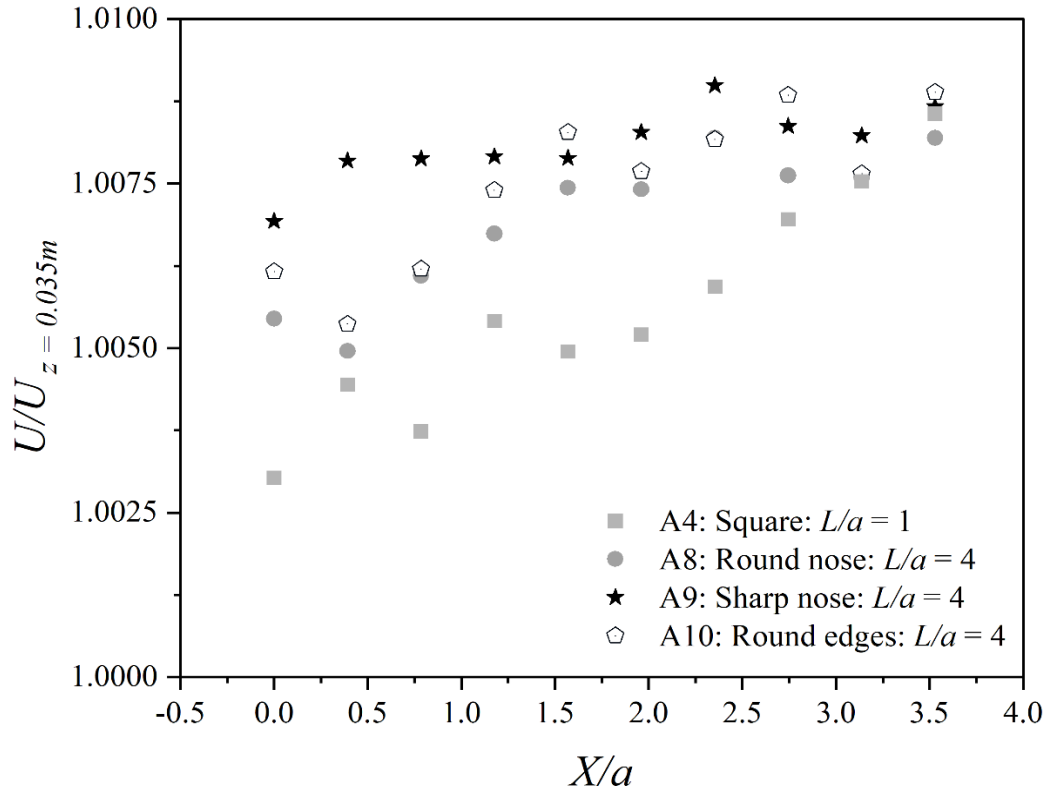


Figure 4.29: Separation velocity profiles for different pier shapes and L/a ratio

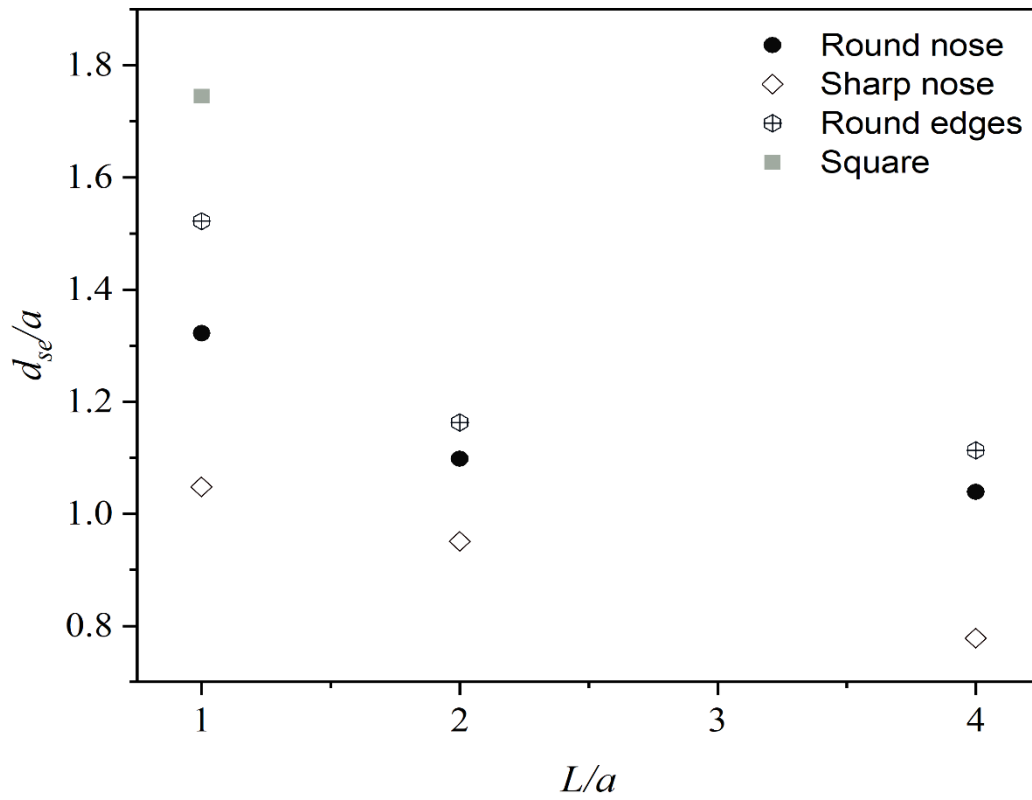


Figure 4.30: Equilibrium scour depth alteration with L/a

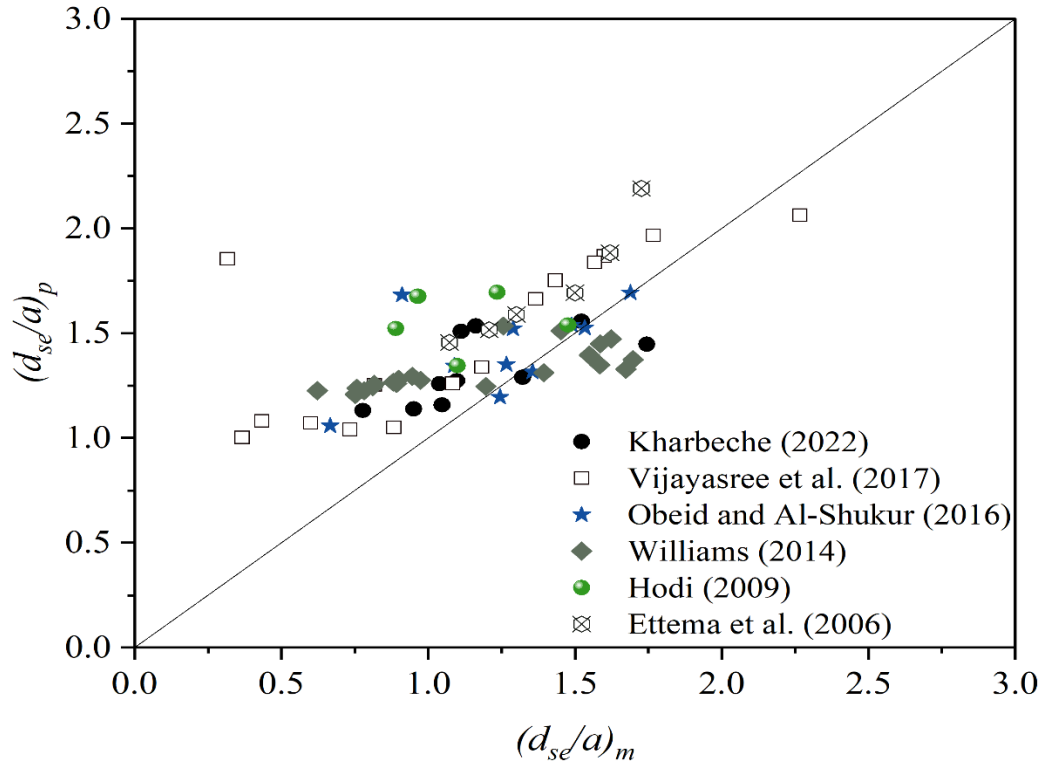


Figure 4.31: Measured vs predicted d_{se}/a values grouped by investigation using Equation 4.7

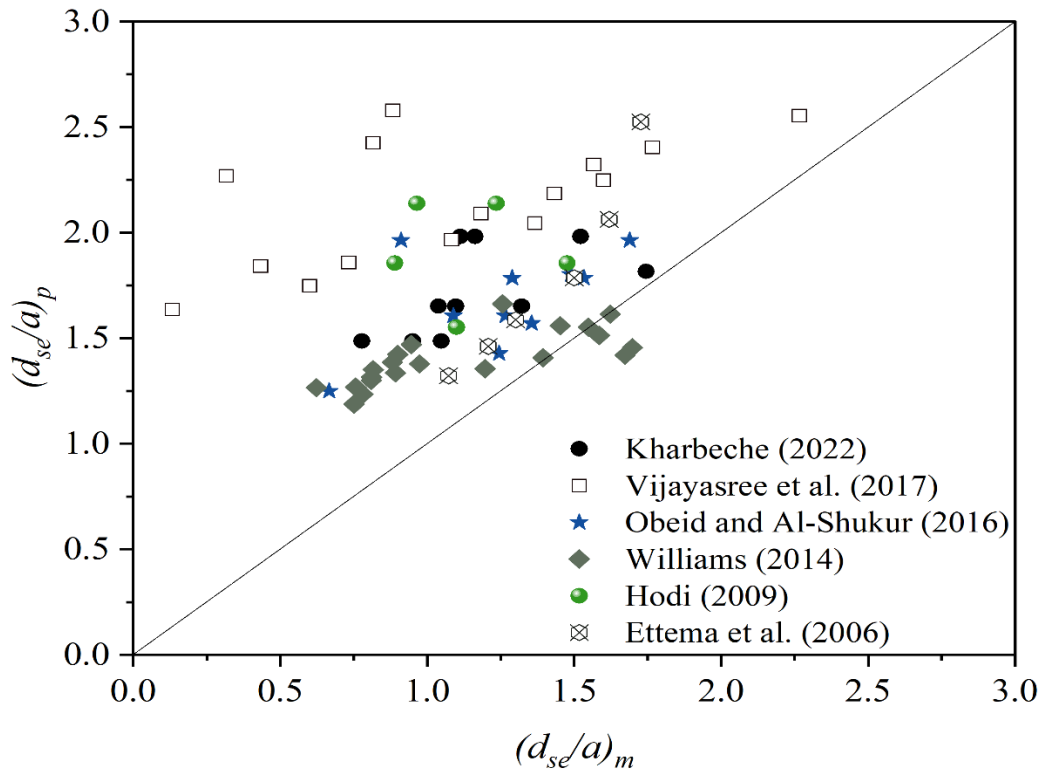


Figure 4.32: Measured vs predicted d_{se}/a values grouped by investigation using HEC-18 equation

CHAPTER 5

CONCLUSIONS AND RECOMMENDATIONS

5.1. Conclusions

The objective of this study was to investigate the pier shape and aspect ratio effects on local scour. Round-nosed, sharp-nosed, and round-edged piers with $L/a = 1, 2,$ and 4 were investigated under the same conditions. Further, scour countermeasure methods were studied by applying five and three sacrificial piles upstream of the main pier in triangular arrangements in order to study their effect on scour depth. Flow measurements were acquired using ADV and LDV to investigate the characteristics of approach flow and flow adjacent to the sides of the cylinder.

In the present investigation, the different parameters affecting scour depth were explored. A new estimation method was developed using the findings of previous investigations carried out at the University of Windsor and two other studies (Ettema et al. 2006, and Vijayasree et al., 2017). The prediction method considers the pier shape and aspect ratio effects on scour depth.

The following conclusions were drawn from the present investigation:

- The pier shape affects the scour depth and geometry. The sharp-nosed pier with $L/a = 4$ recorded the minimum d_{se}/a between all the pier shapes investigated with scour decrease of 25% compared to the round-nosed pier with $L/a = 4$. However, the square pier with $L/a = 1$ resulted in the maximum scour depth with a scour increase of 66% compared to the circular pier with $L/a = 1$.
- The relative scour depth d_{se}/a decreases with increasing the pier aspect ratio. The round-nosed pier with $L/a = 4$ recorded a scour decrease of 21% and 5% compared to the round-nosed piers with $L/a = 1$ and 2 , respectively.
- The use of scour countermeasure helped reduce the scour depth. The scour reduction for the three sacrificial piles was more significant than five sacrificial piles. Further, the scour reduction increases with increasing the L/a ratio. The round-edged pier with $L/a = 4$ with three sacrificial piles recorded the maximum scour reduction, which is equal to 64% in this investigation.
- The separation point and velocity magnitude changed with varying pier shape at the edges of the pier.

- Based on the previous investigations' findings at the University of Windsor, a new scour estimation method was developed, where the pier shape and aspect ratio were incorporated in this method. The trend of the new equation is reasonable to the line of perfect agreement using previous laboratory experimental results. It does not tend to over or under predict the scour depth.

5.2. Recommendations

Further investigations should be made in order to develop a more comprehensive model that describes the effect of pier shape and aspect ratio on scour depth. L/a ratios greater than 4 can be investigated. In addition, more countermeasures should be applied to the different pier shapes to explore the best countermeasure in reducing scour depth. Other parameters affecting scour, such as pier alignment should be studied in the future. Finally, computational fluid dynamics (CFD) application is essential in order to verify the experimental results and refine the proposed scour estimation method.

REFERENCES

1. Azevedo, M. L., Leite, F.C., and Lima, M.M.C.L. (2014). "Experimental study of scour around circular and elongated piers with and without pier slot". *National Conference of Fluid Mechanics, Thermodynamics, and Energy*, Porto, Portugal: MEFTE, 209-2015.
2. Beg, M. (2010). "Characteristics of Developing Scour Holes around Two Piers Placed in Transverse Arrangement" . International Conference on *Scour and Erosion*, San Francisco, USA, 76-85.
3. Breusers, H.N.C., Nicollet, G., and Shen, H.W. (1977). "Local Scour around Cylindrical Piers". *Journal of Hydraulic Research*, 15(3), 211-252.
4. Chabert, J. and Engeldinger, P. (1956). "Study of Scour around Bridge Piers". *Rep. Prepared for the National Laboratory of Hydraulic, Chatou, France*.
5. Chanson, H., Trevethan, M., and Aoki, S. (2005). "*Acoustic Doppler Velocimeter (ADV) in a small estuarine system: Field experience and Despiking*", *Proceeding of 31st Biennial IAHR Congress, Seoul, South Korea, Theme E2, Paper 0161, 3954-3966*.
6. Chavan, R., Venkataramana, B., and Acharya, P. (2018). "Comparison of scour and flow characteristics around circular and oblong bridge piers in seepage affected alluvial channels". *Journal of Marine Science and Application*, 254-264, <https://doi.org/10.1007/s11804-018-0016-6>.
7. Chiew, Y. (1984). "*Local Scour at Bridge Piers*". PhD Thesis, Auckland, New Zealand: School of Engineering, University of Auckland.
8. CTV News. (2013). "*Calgary bridge failure caused by flooding*." Accessed from CTV News, Canada: <https://www.ctvnews.ca/canada/calgary-bridge-failure-caused-by-flooding-cp1.1343758>.
9. D'Alessandro, C. (2013). "*Effect of Blockage on Circular Bridge Pier Local Scour*". M.A.Sc. Thesis, Faculty of Engineering, University of Windsor, Canada.
10. Dargahi, B. (1990). "Controlling Mechanism of local scouring". *Journal of Hydraulic Engineering*, 116(10), 1197-1214.
11. Debnath, K. and Chaudhuri, S. (2012). "Local scour around non-circular piers in clay-sand mixed cohesive sediment beds". *Engineering Geology*, 151, 1-14.
12. Diab, R., Link, O., and Zanke, U. (2010). "Geometry of developing and equilibrium scour holes at bridge piers in gravel" . *Canadian Journal of Civil Engineering* , 37(4), 544-552.
13. Ettema, R., Kirkil, G., and Muste, M. (2006). "Similitude of Large-Scale Turbulence in Experiments on Local Scour at Cylinders". *Journal of Hydraulic Engineering*, 132(1), 33-40 [https://doi.org/10.1061/\(ASCE\)07339429\(2006\)132:7\(635\)](https://doi.org/10.1061/(ASCE)07339429(2006)132:7(635)).
14. Ettema, R., Melville, B.W., and Constantinescu, G. (2011). "*Evaluation of Bridge Scour*

Research: Pier Scour Processes and Predictions". Project 24-27(01), National Cooperative Highway Research Program Web-Only 175. Transportation Research Board of the National Academies: http://onlinepubs.trb.org/onlinepubs/nchrp/nchrp_w175.pdf

15. Figliola, R. and Beasley, D. (2011). *"Theory and Design for Mechanical Measurements: Fifth Edition"*. USA: John Wiley and Sons, Inc.

16. Guo, J. (2012). "Pier Scour in Clear Water for Sediment Mixtures". *Journal of Hydraulic Research*, 50(1), 18-27.

17. Haque, A., Rahman, M., Islam, T., and Hussain, A. (2007). "Scour Mitigation at Bridge Piers using Sacrificial Piles". *International Journal of Sediment Reserve*, 21(1), 49-59.

18. Hodi, B. (2009). *"Effect of blockage and densimetric Froude number on circular bridge pier local scour"*. M.A.Sc. Thesis, Faculty of Engineering, University of Windsor, Canada.

19. Kalkert, C. and Kayser, C. J. (2006). *"Laser Doppler Velocimetry Technique"*. University of San Diego, California.

20. Karim, M and Chang, F.F. (1972). "An Experimental Study of Reducing Scour around Bridge Piers using Piles". *Rep. South Dakota Dept. of Highways*.

21. Kayaturk, S., Kökpinar, M., and Gönüs, M. (2004). "Effect of Collar on Temporal Development of Scour around Bridge Abutment". International Conference of Scour and Erosion (ICSE 2), Singapore, Nanyang Technological University, 14-17.

22. Kharbeche, M., Balachandar, R., and Williams, P. (2021). "Effect of gap width and pile diameter on efficacy of sacrificial piles for scour mitigation". *International Conference on Scour and Erosion*, Washington- DC (To be published).

23. Lagasse, P.F. (2007). *"Countermeasures to Protect Bridge Piers from Scour"*. Washington DC: Transportation Research Board: National Cooperative Highway Research Program (NCHRP) Rep. No. 593.

24. Lima, M. (2014). "Shallow water flow around an elongated bridge pier". *National Conference of Fluid Mechanics, Thermodynamics, and Energy*, Porto, Portugal: MEFTE, 215-221.

25. Masjedi, A., Shafaei Bejestan, M, and Esfandi, A.(2010). "Reduction of Local Scour at a Bridge Pier Fitted with a Collar in a 180 Degree Flume Bend (Case Study: Oblong Pier)". *International Journal of Sediment Research*, 25(2010), 304-312: DOI: 10.1016/S1001-6058(10)60012-1.

26. Melville, B. and Chiew, Y.M. (1999). "Time Scale for Local Scour at Bridge Piers". *Journal of Hydraulic Engineering* , 125(1) 59-65.

27. Melville, B. and Coleman, S. (2000). "Bridge Scour, Colorado". *Water Resources Publication*.

28. Melville, B. and Hadfield, A. (1999). "Use of Sacrificial Piles as Pier Scour Countermeasures". *Journal of Hydraulic Engineering* , 125(11): 1221-1224.
29. Obeid, Z. and Al-Shukur, A.-H. (2016). "Experimental Study of Bridge Pier Shape to Minimize Local Scour". *International Journal of Civil Engineering and Technology*, 7(2016), 162-171.
30. Padgett, J., DesRoches, R., Nielson, B., Yashinsky, M., Kwon, O-S, Burdette, N., and Tavera, Ed. (2008). Bridge damage and repair costs from hurricane Katrina. *Journal of Bridge Engineering*, 13(1): 6-14, DOI: 10.1061/ASCE1084-0702200813:16.
31. Paice, C., Hey, R.D., Whitbread, J., (1993). "Protection of bridge piers from scour". Presented at the bridge management 2: Inspection, maintenance assessment and repair. Papers presented at the second international conference on bridge management held April 1993L 1993, University of Surrey, Guildford, Proc., Hydraulic Engineering Conference, Dubrovnik, Yugoslavia, pp. 1061–1069.
32. Parker, Melville, B., G., Voigt, R.L, and Toro-Escobar, C. (1998). "Countermeasures to Protect Bridge Piers from Scour". Washington, D.C.: User's guide, National Cooperative Highway Research Program, Transportation Research Board, National Research Council.
33. Roy, C. (2017). "Effect of bridge pier geometry on local scour". *International Journal of Earth Sciences and Engineering*, 10(2), 374-377, DOI:10.21276/ijee.2017.10.0234.
34. Shen, H.W., Schneider, V.R., and Karaki, S. (1966). "Mechanics of Local Scour".
35. Tafarojnoruz, A., Gaudio, R., and Colomino, F.(2012). "Evaluation of Flow-Altering Countermeasures against Bridge Pier". *Amercian Society of Civil Engineers*, 138(3): 297-305, doi/10.1061/%28ASCE%29HY.19437900.0000512
36. Tseng, M-H., Yen, C-L., and Song, C.S. (2000). "Computation of three-dimensional flow around square and circular piers". *International Journal for Numerical Methods in Fluids*, 34: 207-227, <https://onlinelibrary.wiley.com/doi/epdf/10.1002/10970363%2820001015%2934%3A3%3C20%3A%3AAID-FLD31%3E3.0.CO%3B2-R>.
37. Vijayasree, B.A, Eldo, T.I., and Ahmad, N. (2017). "Influence of bridge pier shape on flow field and scour geometry". *International Journal of Rivr Basin Management* , 17(1), 109-129, <https://doi.org/10.1080/15715124.2017.1394315>.
38. Wang, H., Tang, H., Liu, Q., and Wang, Y. (2016). "Experimental and Numerical Investigations on the Performance of Sacrificial Piles in Reducing Local Scour around Pile Groups". *National Hazards*, 85(3), 1417-1435.
39. Williams, P. (2014). "Scale effect on design estimation of scour depths at piers". M.A.Sc. Thesis, Faculty of Engineering, University of Windsor, Canada.

40. Williams, P., Bolisetti, T., and Balachandar, R. (2016). "Evaluation of governing parameters on scour geometry". *Canadian Journal of Civil Engineering*, 44(1): 48 - 58.

41. Williams, P. (2019). "The role of approach flow and blockage on local scour around circular cylinders with and without countermeasures". PhD. Thesis, Faculty of Engineering, University of Windsor, Canada.

42. Zarrati, A.R., Nazariha, M., and Mashahir, M.B. (2006). "Reduction of Local Scour in the Vicinity of Bridge Pier Groups using Collars and Riprap. *Journal of Hydraulic Engineering*, 132(2): 154-162.

VITA AUCTORIS

NAME: Mohamed Kharbeche

PLACE OF BIRTH: Bizerte, Tunisia

YEAR OF BIRTH: 1994

EDUCATION: Hedi Chaker High School
Bizerte, Tunisia
2009- 2014

National Engineering School of Tunis
Tunis, Tunisia
2015-2019

University of Windsor, M.A.Sc.
Windsor, ON
2020-2022